Secondary Organic Aerosol (SOA) Formation from the β-pinene+NO_3 System: Effect of Humidity and Peroxy Radical Fate

C. M. Boyd[1]; J. Sanchez[1]; L. Xu[1]; A. J. Eugene[2]; T. Nah[1]; W. Y. Tuet[1]; M. I. Guzman[2]; N. L. Ng[1,3*]

[1]School of Chemical and Biomolecular Engineering, Georgia Institute of Technology, Atlanta, GA 30332, USA

[2]Department of Chemistry, University of Kentucky, Lexington, KY 40506, USA

[3]School of Earth and Atmospheric Sciences, Georgia Institute of Technology, Atlanta, GA 30332, USA

[*]Correspondence to: Nga Lee Ng (ng@chbe.gatech.edu)

Abstract

The formation of secondary organic aerosol (SOA) from the oxidation of β-pinene via nitrate radicals is investigated in the Georgia Tech Environmental Chamber facility (GTEC). Aerosol yields are determined for experiments performed under both dry (RH < 2%) and humid (RH = 50% and RH = 70%) conditions. To probe the effects of peroxy radical (RO_2) fate on aerosol formation, "RO_2+NO_3 dominant" and "RO_2+HO_2 dominant" experiments are performed. Gas-phase organic nitrate species (with molecular weights of 215 amu, 229 amu, 231 amu, and 245 amu) are detected by chemical ionization mass spectrometry and their formation mechanisms are proposed. The NO^+ (at *m/z* 30) and NO_2^+ (at *m/z* 46) ions contribute about 11% to the combined organics and nitrate signals in the typical aerosol mass spectrum, with NO^+:NO_2^+ ratio ranging from 4.8 to 10.2 in all experiments conducted. The SOA yields in the "RO_2+NO_3 dominant" and "RO_2+HO_2 dominant" experiments are comparable. For a wide range of organic mass loadings (5.1-216.1 μg m^{-3}), the aerosol mass yield is calculated to be 27.0-104.1%. Although humidity does not appear to affect SOA yields, there is evidence of particle-phase hydrolysis of organic nitrates, which are estimated to compose 45-74% of the organic aerosol. The extent of organic nitrate hydrolysis is significantly lower than that observed in previous studies on photooxidation of volatile organic compounds in the presence of NO_x. It is estimated that about 90 and 10% of the organic nitrates formed from the β-pinene+NO_3 reaction are primary organic nitrates and tertiary organic nitrates, respectively. While the primary organic nitrates do not appear to hydrolyze, the tertiary organic nitrates undergo hydrolysis with a lifetime of 3-4.5 hours. Results from this laboratory chamber study provide the fundamental data to evaluate the contributions of monoterpene+NO_3 reaction to ambient organic aerosol measured in the southeastern United States, including the Southern Oxidant and Aerosol Study (SOAS) and the Southeastern Center for Air Pollution and Epidemiology (SCAPE) study.

1) Introduction

Owing to their high emissions and high reactivity with the major atmospheric oxidants (O_3, OH, NO_3), the oxidation of biogenic volatile organic compounds (BVOCs) emitted by vegetation, such as isoprene (C_5H_8), monoterpenes ($C_{10}H_{16}$), and sesquiterpenes ($C_{15}H_{24}$), is believed to be the dominant contributor to global secondary organic aerosol (SOA) formation (e.g., Kanakidou et al., 2005). While this is supported by the observation that ambient organic aerosol is predominantly "modern" and therefore biogenic in origin (Lewis et al., 2004; Schichtel et al., 2008; Marley et al., 2009), there exists an apparent contradiction because ambient organic aerosol is well-correlated with anthropogenic tracers (de Gouw et al., 2005; Weber et al., 2007). This apparent discrepancy could be reconciled if anthropogenic pollution influences the atmospheric oxidation of BVOCs and their aerosol formation pathways. The oxidation of BVOCs by nitrate radicals (NO_3), formed from the reaction of ozone with NO_2, provides a direct link between anthropogenic pollution and the abundance of biogenic carbon in atmospheric aerosol.

Biogenic hydrocarbons react rapidly with nitrate radicals (Atkinson and Arey, 2003b) and the secondary organic aerosol (SOA) yields are generally higher than in photooxidation and ozonolysis (e.g., Griffin et al., 1999; Hallquist et al., 1999; Spittler et al., 2006; Ng et al., 2008; Fry et al., 2009; Rollins et al., 2009; Fry et al., 2011; Fry et al., 2014). As monoterpene emissions are not entirely light-dependent, they are emitted during the day and at night (Fuentes et al., 2000; Guenther et al., 2012) and can contribute substantially to ambient organic aerosol. Monoterpenes have also been found to make up as much as 28% of non-methane organic carbon emissions from biomass burning in both field and laboratory studies (Akagi et al., 2013; Hatch et al., 2015; Stockwell et al., 2015). Fires from biomass burning are more likely to smolder at night and are therefore more likely to emit monoterpenes, which can then react with nitrate radicals (Akagi et al., 2013). Results from previous field studies provided evidence of aerosol formation from nitrate radical oxidation of BVOCs during both daytime and nighttime (McLaren et al., 2004; Iinuma et al., 2007; Fuentes et al., 2007; Brown et al., 2009; Rastogi et al., 2011; Rollins et al., 2012; Brown et al., 2013; Rollins et al., 2013). Specifically, many of these studies found a significant increase in the amount of monoterpene organic aerosol and oxidation products at

night, which could be attributed to nighttime monoterpene oxidation by nitrate radicals (McLaren et al., 2004; Iinuma et al., 2007; Rastogi et al., 2011). Results from recent flight measurements in Houston, TX also showed that organic aerosol was enhanced in the nocturnal boundary layer at levels in excess of those attributable to primary emissions, implying a source of SOA from the BVOCs+NO_3 reaction (Brown et al., 2013).

Global modeling studies showed large variations in the total SOA burden that can be attributed to the oxidation of BVOCs by nitrate radicals, ranging from ~5 to 21% (Hoyle et al., 2007; Pye et al., 2010). Specifically, Pye et al. (2010) showed that the inclusion of nitrate radical oxidation reaction doubled the total amount of terpene (monoterpenes and sesquiterpenes) aerosol, pointing to the significant contribution of this chemistry to total organic aerosol burden. In these modeling studies, all aerosol formation from the nitrate radical oxidation of terpenes was calculated based on the β-pinene+NO_3 SOA yields obtained in Griffin et al. (1999). A recent modeling study by Russell and Allen (2005) determined that as much as 20% of all nighttime SOA is from the reaction of β-pinene+NO_3. Due to the significance of nitrate radical oxidation pathway in SOA formation, it is important that the SOA yields for BVOCs+NO_3, and especially that of β-pinene+NO_3, are well-constrained from fundamental laboratory studies and accurately represented in models.

The majority of the previous laboratory studies of the BVOCs+NO_3 chemistry were performed under dry conditions (Berndt and Boge, 1997a, b; Wängberg et al., 1997; Griffin et al., 1999; Hallquist et al., 1999; Bonn and Moorgat, 2002; Spittler et al., 2006; Ng et al., 2008; Rollins et al., 2009; Fry et al., 2009; Perraud et al., 2010; Fry et al., 2011; Kwan et al., 2012; Jaoui et al., 2013; Fry et al., 2014). The effect of relative humidity on SOA formation, however, could potentially be important for nighttime (where NO_3 radicals dominate) and early morning chemistry as the ambient RH is typically higher at these times. Several recent studies have investigated the effect of water on SOA formation from the nitrate radical oxidation pathway but the results are inconclusive. For instance, Spittler et al. (2006) found that the SOA yield is lower at 20% RH compared to dry conditions, suggesting that water vapor may alter the gas-phase oxidation mechanism and/or partitioning into the particle phase, thus shifting the equilibrium partitioning of organic compounds. However, other studies showed that the presence of water

vapor did not affect particle size distributions and SOA formation (Bonn and Moorgat, 2002; Fry et al., 2009). Thus, the role of water in SOA formation from nitrate radical oxidation of BVOCs is still unclear.

Another important parameter in SOA formation from BVOCs+NO_3 is the fate of peroxy radicals, which directly determines the oxidation products, SOA yields, and aerosol chemical and physical properties (Kroll and Seinfeld, 2008; Orlando and Tyndall, 2012; Ziemann and Atkinson, 2012). Previous studies regarding the effects of peroxy radical fates on SOA formation from BVOCs typically focused on photooxidation and ozonolysis systems (e.g., Presto et al., 2005; Kroll et al., 2006; Ng et al., 2007b; Eddingsaas et al., 2012; Xu et al., 2014) and isoprene+NO_3 chemistry (Kwan et al., 2012; Ng et al., 2008; Nguyen et al., 2014). To our knowledge, the effects of differing peroxy radical branching on SOA formation from nitrate radical oxidation of monoterpenes have not been investigated. The relative importance of different peroxy radical reaction channels concerning BVOCs+NO_3 chemistry in the atmosphere is not well established (Brown and Stutz, 2012). While earlier studies by Kirchner and Stockwell (1996) suggested that RO_2+NO_3 is more important in the nighttime atmosphere, a recent study by Mao et al. (2012) showed that the HO_2 mixing ratios are often on the order of 10 ppt at night. It is therefore possible that RO_2+HO_2 pathway could be an important pathway in nighttime oxidation of BVOCs.

Nitrate radical chemistry is expected to produce a substantial amount of organic nitrate compounds, owing to direct addition of nitrate radical via reaction with a double bond. Organic nitrates have been observed to form a substantial portion of atmospheric aerosol in field studies (Brown et al., 2009; Day et al., 2010; Zaveri et al., 2010; Beaver et al., 2012; Rollins et al., 2012; Fry et al., 2013; Rollins et al., 2013; Brown et al., 2013; Xu et al., 2015a). Organic nitrate formation has a significant impact on total NO_x lifetime, especially in NO_x-limited regions where NO_x lifetime is sensitive to the formation rates of organic nitrates (Browne and Cohen, 2012). Ambient organic nitrates can be formed through photooxidation of VOCs in the presence of NO_x (Chen et al., 1998; Arey et al., 2001; Yu et al., 2008) and through nitrate radical addition (Spittler et al., 2006; Perring et al., 2009; Rollins et al., 2009; Kwan et al., 2012). One removal mechanism for atmospheric organic nitrates is hydrolysis in the particle phase (e.g., Sato, 2008;

Szmigielski et al., 2010; Darer et al., 2011; Hu et al., 2011; Liu et al., 2012; Rindelaub et al., 2015). Modeling studies have assumed that the majority (75%) of the organic nitrates formed in the day are composed of tertiary nitrates based on results from the photooxidation of α-pinene and β-pinene in the presence of NO_x (Browne et al., 2013). However, the organic nitrates formed from photooxidation and nitrate radical oxidation could have different chemical structures (primary, secondary, and tertiary) and need to be investigated to better constrain the fates of organic nitrates (e.g., hydrolysis lifetime) in the atmosphere over their entire life cycle (both day and night).

The goal of this study is to determine the aerosol yields and characterize the mechanisms and chemical composition of SOA formation from the β-pinene+NO_3 system. Laboratory chamber experiments are performed in the dark under dry and humid conditions. To investigate the effects of peroxy radical fates on SOA yields and chemical composition, the experiments are designed to probe the "RO_2+NO_3" vs. "RO_2+HO_2" reaction pathways. Aerosol yields are obtained over a wide range of initial β-pinene mixing ratios. Based on the measured gas-phase and particle-phase oxidation products, mechanisms for SOA formation from β-pinene+NO_3 are proposed. Results from this study are used to evaluate the contributions of nitrate radical oxidation of monoterpenes to ambient organic aerosol measured in the southeastern United States (US), including the Southern Oxidant and Aerosol Study (SOAS) and the Southeastern Center for Air Pollution and Epidemiology (SCAPE) study.

2) Experimental

2.1) Laboratory Chamber Experiments

All experiments are performed in the Georgia Tech Environmental Chamber facility (GTEC), which consists of two 12 m^3 flexible Teflon (FEP 2 mil) chambers suspended in a 21 ft. x 12 ft. temperature-controlled enclosure. The full operational temperature range of the facility is 4–40 ±0.5 ^oC. A schematic of the chamber facility is shown in Fig. 1. Each of the chambers has three Teflon manifolds with multiple sampling ports. Ports allow for the introduction of clean air, gas-phase reagents, seed aerosol, and for measurements of RH, temperature, gas-phase composition, and particle-phase composition. The chambers are surrounded by blacklights (Sylvania, 24922)

with output predominately in the ultraviolet region between 300 nm and 400 nm, with a maximum at 354 nm. The blacklights are supplemented by natural sunshine fluorescent lights (Sylvania, 24477), which have wavelengths between 300 nm to 900 nm. The j_{NO2} of the chamber facility is 0.28 min^{-1} when all of the blacklights are turned on.

Experimental conditions are summarized in Table 1. Prior to each experiment, the chambers are cleaned by flowing pure air (generated from AADCO, 747-14) for at least 24 hours at a rate of 40 LPM, or equivalent to 0.2 chamber volumes per hour. This ensures that the ozone, NO, and NO_2 concentrations are less than 1 ppb and the particle concentration is lower than 10 cm^{-3}. Experiments are performed in the dark under either dry (RH < 2%) or humid (RH = 50%, 70%) conditions. The air is humidified by passing pure air through bubblers prior to introduction into the chamber. The temperature and humidity inside each Teflon chamber are measured using a hygrothermometer (Vaisala, HMP110). Seed aerosol is generated by atomizing an ammonium sulfate solution (8 mM) or an ammonium sulfate/sulfuric acid mixture ($[(NH_4)_2SO_4]$:$[H_2SO_4]$ = 3:5, molar ratio) into the chamber. The seed number and mass concentrations prior to typical experiments are approximately 2.0×10^4 cm^{-3} and 30 μg m^{-3}. The pH of the $(NH_4)_2SO_4$ seed and $(NH_4)_2SO_4$+H_2SO_4 seed at RH = 50% is about 4.6 and 2.4, respectively, based on calculations from prior studies (Gao et al., 2004). Nucleation experiments are performed under both dry and humid (RH = 50%, 70%) conditions to determine organic aerosol density and characterize vapor wall loss effects on SOA yields. All experiments are performed at 298 K.

Experiments are designed to probe the effects of peroxy radical chemistry (RO_2+HO_2 vs. RO_2+NO_3) on SOA formation from the reaction of β-pinene with nitrate radicals. The procedure for chemical injection depends on the desired fate of the peroxy radicals in the experiments. To enhance the branching ratio of RO_2+HO_2 in the chamber experiments, formaldehyde is first added to the chamber (Nguyen et al., 2014). Formalin solution (Sigma-Aldrich, 37% HCHO) is injected into a glass bulb and clean air is passed over the solution until it evaporates. After this, seed aerosol, NO_2 (Matheson, 500 ppm), and ozone (generated by passing zero air through a UV radiation cell, Jelight 610) are injected into the chamber. NO_2 and O_3 concentrations are chosen ($[NO_2]$:$[O_3]$ ≈ 4:3) to ensure that 99% of the β-pinene reacts with nitrate radicals instead of

ozone. The NO_2 and O_3 react to form nitrate radicals and subsequently N_2O_5 through the following reactions:

$$NO_2 + O_3 \rightarrow NO_3 + O_2 \quad \text{(R1)}$$

$$NO_3 + NO_2 \leftrightarrow N_2O_5 \quad \text{(R2)}$$

Formaldehyde then reacts with nitrate radicals to form HO_2 radicals via the following reaction:

$$HCHO + NO_3 + O_2 \rightarrow HNO_3 + CO + HO_2 \quad \text{(R3)}$$

Enough formaldehyde (3-22 ppm) is added to the chamber to ensure that the RO_2+HO_2 radical branching ratio is an order of magnitude higher than the RO_2+RO_2 and RO_2+NO_3 pathways (Supplement). The chamber content is allowed to mix for ~30 minutes, after which a desired amount of β-pinene is injected into a glass bulb, where it is introduced into the chamber by passing clean air through the glass bulb. Introduction of β-pinene into the chamber marks the beginning of the experiment. We refer to this set of experiments as "RO_2+HO_2 dominant" experiments.

For "RO_2+NO_3 dominant" experiments, seed aerosol is first introduced into the chamber, followed by β-pinene injection. After allowing ~30 minutes for the β-pinene concentration to stabilize, N_2O_5 is injected into the chamber. To generate N_2O_5, a mixture of NO_2 and O_3 is pre-reacted in a flow tube (flow rate = 1.3 LPM, residence time = 71 sec) before entering the chamber. The N_2O_5 concentration is estimated by modeling the reaction of NO_2 and O_3 in the flow tube. For this set of experiments, the introduction of N_2O_5 marks the beginning of the experiment. We aim for an initial N_2O_5:β-pinene ratio of ~6:1. It is noted that the ozone concentration in the chamber is sufficiently low that at least 99% of β-pinene reacts with nitrate radicals. N_2O_5 continuously dissociates to form NO_2 and nitrate radicals during the experiment to reestablish equilibrium as the nitrate radicals react with β-pinene. The high initial N_2O_5 and nitrate radical concentrations relative to β-pinene favor the RO_2+NO_3 pathway.

For all experiments except "RO_2+HO_2 dominant" experiments conducted under humid conditions (RH = 50%, 70%), a Gas Chromatograph-Flame Ionization Detector (GC-FID, Agilent 6780A) measures a β-pinene concentration of zero (below detection limit) within the first scan (scan time = 11.7 min) after the experiment begins. This suggests that β-pinene is completely consumed within 11.7 minutes of N_2O_5 injection for the "RO_2+NO_3 dominant" experiments and that β-pinene is fully reacted away before being detected by the GC-FID in the "RO_2+HO_2 dominant" experiments under dry conditions. The concentration of β-pinene is calculated from the mass of the hydrocarbon injected and the volume of the chamber. The chamber volume is determined to be approximately 12 m^3 by injecting a known volume of NO_2 standard (Matheson, 500 ppm) into the chamber and measuring the resulting NO_2 concentration inside the chamber.

Ozone and NO_x concentrations are monitored with an O_3 Analyzer (Teledyne T400) and an ultrasensitive chemiluminescence NO_x monitor (Teledyne 200EU), respectively. Total aerosol volume and size distributions are measured with a Scanning Mobility Particle Sizer (SMPS, TSI). The SMPS consists of a differential mobility analyzer (DMA) (TSI 3040) and Condensation Particle Counter (CPC) (TSI 3775). Bulk particle chemical composition is measured with an Aerodyne High Resolution Time-of-Flight Aerosol Mass Spectrometer (HR-ToF-AMS). The working principle and operation of the HR-ToF-AMS are described in detail elsewhere (DeCarlo et al., 2006). The HR-ToF-AMS provides quantitative measurements of organics, nitrate, sulfate, ammonium, and chloride. Elemental analysis are performed on the data to determine elemental composition (e.g., O:C, N:C ratios) of the bulk aerosol (Canagaratna et al., 2015).

A suite of gas-phase oxidation products and N_2O_5 are measured using a Quadrupole Chemical Ionization Mass Spectrometer (CIMS) with I^- as the reagent ion, which has high selectivity towards reactive nitrogen species, peroxides, and carboxylic acids (Huey, 2007; McNeill et al., 2007; Zhao et al., 2012). The CIMS uses methyl iodide to produce I^- ions that ionize gas-phase products through association (Slusher et al., 2004; Zheng et al., 2011). It has been shown that I^- addition to gas-phase molecules provides a molecule-iodide adduct that preserves the original species of the compounds being sampled. The gas-phase species are detected as *m/z* = MW+127.

Masses with specific *m/z* are selected for detection using a quadrupole mass filter. These species are then detected by an electron multiplier which amplifies incident charge through secondary electron emission to produce a measurable current that scales with gas-phase concentration. Due to unavailability of standards for the oxidation products, the instrument is not calibrated for these compounds and concentrations are not reported. However, the CIMS data allow for identification and comparison of the abundance of specific gas-phase oxidation products formed in different experimental conditions.

2.2) Analysis of Particle-Phase Products

Aerosol samples are collected on Teflon filters (Pall Corp. R2PL047, 1-μm pore size and 47-mm diameter) during the SOA experiments (Experiments 9, 10, 22, 23, 32, 33 in Table 1) and for a series of blank/control experiments. These blank experiments are 1) clean chamber (no aerosol) at RH < 2%, 2) clean chamber (no aerosol) at RH = 50%, 3) clean chamber at RH =50% with only N_2O_5 injected, and 4) clean chamber at RH < 2% with only β-pinene injected. All filters collected during the chamber experiments and controls are stored at a temperature below −20°C before sample extraction and preparation for chromatographic analysis.

Each filter is extracted twice by sonication (Branson 3510) for 15 min in 2.50 mL acetonitrile (Fisher Optima, LC-MS grade). After combining both aliquots, each extracted sample is blown dry under a gentle stream of nitrogen (Scott-Gross, UHP), reconstituted with 1000 μL acetonitrile, and transferred to a chromatographic vial. Samples are analyzed with an Accela (Thermo Fisher Scientific) ultra-high-performance liquid chromatographer (UHPLC) equipped with a 1250 quaternary delivery pump, a photodiode array detector (PDA) with a 5-cm LightPipe flow cell, and a mass spectrometry (MS) detector (Thermo MSQ Plus). Samples are injected (50 μL) with an Accela autosampler into the reversed-phase chromatographic column (Hypersil gold C18, 50 × 2.1 mm, 1.9 μm particle size, Thermo Scientific). Excalibur software is used to control the UHPLC-PDA-MS system. Chromatographic separation at a constant flow rate of 800 μL min^{-1} from 0 to 1 min is isocratic with 90% (A) 0.10 mM formic acid (Fisher Optima, LC-MS grade) in ultrapure water (18.2 MΩ cm Purelab Flex, Veolia) and 10% (B) 0.10 mM formic acid in acetonitrile. Gradient elution from 1 to 8 min reaches a 10:90 ratio of solvents A:B and remain

isocratic from 8 to 10 min. Selected chromatograms utilize 0.4-1.0 mM acetic acid (Acros, glacial ACS, 100.0% by assay) instead of 0.1 mM formic acid in the mobile phase. After the PDA registered the UV–visible spectra from 190 to 700 nm, the flow is interfaced with an electrospray ionization (ESI) probe (1.9 kV needle voltage, 350°C probe temperature, and 70 psi N_2 nebulizing gas) to the MS detector set to detect negative ions in the range of *m/z* 50 to 650 amu. Selected samples are analyzed under variable cone voltage (10-100 V) to register the fragmentation pattern of the peaks and gain structural information of the products. The extraction method shows an efficient 98.8% recovery, when 98.6 μg of 4-nitrophenol (Acros, 98.0%) are spiked onto a blank filter.

3) Results

Gas-phase oxidation and aerosol growth is observed to be a rapid process in the β-pinene+NO_3 reaction. Peak aerosol growth is typically observed within 10-15 minutes for all reaction conditions except in humid (RH= 50%, 70%) "RO_2+HO_2 dominant" experiments, where aerosol reaches peak growth in about 30 minutes. Figure S1 shows a typical mass spectrum for the CIMS data. Specifically, the major gas-phase products are detected at *m/z* 342, 356, 358, and 372 (which correspond to MW = 215 amu, 229 amu, 231 amu, 245 amu, respectively). These compounds likely correspond to organic nitrate species. Figure 2 shows the time series of these species and the aerosol growth over the course of a typical "RO_2+HO_2 dominant" experiment in dry conditions. The products at *m/z* 356 and 358 (MW = 229 amu and 231 amu) decrease over the course of the experiment. While this can be attributed to vapor phase wall loss, it is also possible that these gas-phase compounds undergo further reaction. This is further supported by the increase in the species at *m/z* 372 (MW = 245 amu). The proposed gas-phase oxidation mechanism and formation of compounds at *m/z* 372 from compounds at *m/z* 356 will be discussed further in Section 4.1.

Although all the above gas-phase species are observed under all reaction conditions, *m/z* 358 (MW = 231 amu) is significantly higher in the "RO_2+HO_2 dominant" experiments than in the "RO_2+NO_3 dominant" experiments (Fig. S2), which is indicative of differences in the gas-phase chemistry depending on the RO_2 fate. Under both "RO_2+HO_2 dominant" and "RO_2+NO_3

dominant" conditions, experiments conducted under dry conditions have significantly higher N_2O_5 concentrations than humid conditions (by at least a factor of 2) as measured by CIMS. This is likely due to N_2O_5 uptake (loss) on the wet chamber surfaces and/or seed aerosol. The relative abundance of N_2O_5 under different experimental conditions is important in terms of β-pinene reaction rate and aging of aerosol, which are discussed in Sections 4.2.2 and 4.4, respectively.

All SOA growth data are corrected for particle wall loss by applying size-dependent wall loss coefficients determined from wall loss experiments at GTEC following the methodology described in Keywood et al. (2004). The size-dependent particle wall loss rates calculated for both chambers at GTEC are shown in Fig. S3. Figures 3 and 4 show the SOA yields for "RO_2+NO_3 dominant" and "RO_2+HO_2 dominant" experiments over a wide range of aerosol mass loadings (ΔM_o = 5.1-216.1 μg m^{-3}). The SOA yields lie in the range of 27.0-104.1% over the conditions studied. Aerosol mass yield (Y) is defined as the aerosol mass concentration produced (ΔM_o) divided by the mass concentration of hydrocarbon reacted (ΔHC), $Y = \Delta M_o/\Delta HC$ (Odum et al., 1996; Bowman et al., 1997; Odum et al., 1997a; Odum et al., 1997b). For all experiments, aerosol mass concentration is obtained from the SMPS aerosol volume concentration (averaged over 30 min at peak growth) and the calculated aerosol density. The aerosol density is calculated from the SMPS volume distribution and the HR-ToF-AMS mass distribution in the nucleation experiments (Bahreini et al., 2005). The densities of the organic aerosol generated in nucleation experiments under dry and humid (RH = 50%, 70%) conditions are determined to be 1.41 g cm^{-3} and 1.45 g cm^{-3} for the "RO_2+NO_3 dominant" experiments and 1.54 g cm^{-3} and 1.61 g cm^{-3} for the "RO_2+HO_2 dominant" experiments.

It can be seen from Fig. 3 that the aerosol yields in the "RO_2+NO_3 dominant" experiments under dry vs. humid conditions in the presence of $(NH_4)_2SO_4$ seed are similar. The presence of the more acidic $(NH_4)_2SO_4$+H_2SO_4 seed does not appear to enhance SOA production in the "RO_2+NO_3 dominant" experiments (Fig. S4). Therefore, we fit the Odum two-product model (Odum et al., 1996; Odum et al., 1997b) to all of our experimental data shown in Fig. 3 to obtain a single yield curve. The SOA yield parameters are given in Table 2. Shown in Fig. 4 are the aerosol yields from "RO_2+HO_2 dominant" experiments under dry vs. humid (RH = 70%)

conditions. The SOA yield curve (solid red line) for the "RO_2+NO_3 dominant" experiments is also shown for comparison.

For comparison, SOA yields from previous β-pinene+NO_3 laboratory chamber studies (Griffin et al., 1999; Fry et al., 2009) are also shown in Fig. 3. Without adding HCHO as an additional HO_2 source, it is likely that the experiments in Griffin et al. (1999) and Fry et al. (2009) are more similar to our "RO_2+NO_3 dominant" experiments. Specifically, Fry et al. (2009) noted that the β-pinene+NO_3 reaction likely does not produce significant concentrations of HO_2 radicals and therefore have a low HO_2/RO_2 ratio. As Griffin et al. (1999) assumed an aerosol density of 1.0 g cm^{-3}, the experimental data from Griffin et al. (1999) shown in Fig. 3 has been multiplied by the density calculated in our study for "RO_2+NO_3 dominant" experiments under dry conditions (i.e., 1.41 g cm^{-3}). The data shown in Fig. 3 from Fry et al. (2009) have also incorporated a particle density of 1.6 g cm^{-3} calculated in their study. In addition to correcting for density, the yield curve partitioning coefficient, K, from Griffin et al. (1999) has been adjusted from 306K to 298K using an enthalpy of vaporization of 42 kJ mol^{-1} for comparison to results from our study (Chung and Seinfeld, 2002). It is noted that the SOA yields obtained in the current study are higher than those in Griffin et al. (1999) and Fry et al. (2009), particularly at lower aerosol mass loadings that are more relevant to ambient environments. These results are discussed in more detail in Section 4.2.

Bulk aerosol composition from the experiments is characterized by the HR-ToF-AMS. A typical high-resolution mass spectrum for aerosol formed under dry conditions where the RO_2+NO_3 pathway is dominant (Experiment 5 in Table 1) is shown in Fig. 5. A key feature of the mass spectrum is the high intensity of the nitrate ions at NO^+ and NO_2^+, which make up about 11% of the combined organics and nitrate signals. The majority (> 90%) of the nitrogen atoms is detected at these two ions with the remaining nitrogen-containing ions detected at higher masses as $C_xH_yO_zN$. The mass spectra for the aerosol generated in the "RO_2+HO_2 dominant" and "RO_2+NO_3 dominant" experiments are similar. One notable difference between the "RO_2+HO_2 dominant" and "RO_2+NO_3 dominant" experiments is the NO^+:NO_2^+ ratio for the organic nitrates (R-ON), which ranges from 4.8-10.2 in all experiments. While the NO^+:NO_2^+ ratio averages 6.5 for "RO_2+NO_3 dominant" experiments, it averages 8.6 for "RO_2+HO_2 dominant" experiments.

Since the values of R-ON may depend on the instrument, we normalize the R-ON to the NO^+:NO_2^+ of ammonium nitrate (R-AN), which is expected to be a better metric (Farmer et al., 2010). In our study, multiple measurements of R-AN are obtained from the ionization efficiency (IE) calibrations and the average value is about 1.8 (range of 1.2-2.7). Applying the nearest R-AN measured to each experiment, we calculate the average R-ON:R-AN ratio to be 3.2 for "RO_2+NO_3 dominant" experiments and 4.8 for "RO_2+HO_2 dominant" experiments.

For both types of experiments, there is a negligible difference in the mass spectrum of the aerosol produced in dry or high humidity (RH = 50%, 70%) conditions. In Fig. 5, nitrate and organic ions are each assigned a different color to indicate an individual AMS HR ion family. There are a few notable ions in the aerosol mass spectrum. The signals at *m/z* 67 ($C_5H_7^+$) and *m/z* 91 ($C_7H_7^+$), while not significant in the high resolution mass spectra of several biogenic SOA systems (Ng et al., 2008; Chhabra et al., 2010), are relatively large for β-pinene+NO_3 SOA. These ions also make up a larger fraction of the HR-ToF-AMS signal for SOA formed from the ozonolysis of β-caryophyllene (Chen et al., 2015) when compared to other biogenic SOA. Therefore, *m/z* 67 ($C_5H_7^+$) and *m/z* 91 ($C_7H_7^+$) could potentially serve as useful indicators for SOA formed from monoterpene/sesquiterpene oxidation in ambient aerosol mass spectra. However, more studies of SOA formed from the oxidation of biogenic VOCs are necessary to apportion ambient OA based on these fragments.

Figure 6 shows the time evolution of the major organic families relative to sulfate measured by the HR-ToF-AMS for a typical dry "RO_2+NO_3 dominant" experiment (Experiment 5 in Table 1). Sulfate is used to normalize the decay of the organic families because it is non-volatile and any decrease in sulfate is reflective of particle wall loss and changes in aerosol collection efficiency (CE) in the HR-ToF-AMS (Henry and Donahue, 2012). Any change of each organic family relative to sulfate is therefore interpreted as a change in organic mass unrelated to particle wall loss or CE. Non-oxidized fragments (CH family in green) decrease more rapidly relative to sulfate than the more oxidized fragments (CHO1 family in purple, CHOgt1 "fragments with greater than 1 oxygen atom" family in pink). The change in mass for each organic family is determined over a 2.5 hour period following peak aerosol growth (at t ~ 15 min) in each "RO_2+NO_3 dominant" experiment (dry and humid). We find that the CHOgt1 family increases

by 4% in dry experiments and remains relatively constant in humid experiments. This is consistent with a larger extent of aerosol aging in the dry experiments and is further discussed in Section 4.4.

Figure 7 shows the time evolution of HR-ToF-AMS nitrate-to-organics ratio in the "RO_2+NO_3 dominant" experiments at RH = 50% normalized by that in the corresponding dry experiments with the same initial hydrocarbon concentration. For simplicity, we refer to this ratio as $(Nitrate:Org)_{norm}$. Normalizing the nitrate-to-organics ratio obtained from the humid experiments to the dry experiments allow for determining the extent of possible organic nitrate hydrolysis under humid conditions. Since only the relative change in the $(Nitrate:Org)_{norm}$ ratio is important for comparison purposes, the maximum $(Nitrate:Org)_{norm}$ measurement for each experiment is set to be unity. Nitrate mass is defined here as the sum of the mass of the NO^+ and NO_2^+ ions. This does not account for the $C_xH_yO_zN$ fragments, but these fragments only account for less than 10% (by mass) of the nitrate functional groups detected by HR-ToF-AMS. As the experiment progresses, the $(Nitrate:Org)_{norm}$ ratio decreases and stabilizes at a value of about 0.9, indicating that there is no further decrease in the mass of nitrate relative to the mass of organics beyond this point. From our particle wall loss experiments, we establish that the particles are lost to the chamber wall with comparable rates under dry and humid conditions, suggesting that the observed decrease in the $(Nitrate:Org)_{norm}$ ratio is not a result of differing particle wall loss in dry and humid experiments. Instead, the decrease under humid conditions is attributed to hydrolysis of organic nitrate compounds in the particle phase. This is further discussed in Section 4.3.2.

4) Discussion

4.1) Proposed Mechanisms

Figure 8 shows the proposed scheme for the generation of species observed by CIMS and UHPLC-PDA-MS analyses from the oxidation of β-pinene with nitrate radicals. The oxidation process starts with Reaction (R1) for the sterically preferred addition of nitrate radical to the primary carbon (C_1) in the double bond of β-pinene (Wayne et al., 1991). The tertiary alkyl radical formed on C_2 can undergo 1) addition of O_2 to form a peroxy radical via Reaction (R2)

(Atkinson and Arey, 2003a), 2) a 1,5-CH_3 shift indicated by Reaction (R3) (Miller, 2003) and, 3) rearrangement via Reaction (R4) (Stolle et al., 2009; Schröder et al., 2010). Reaction (R4) is thought to be a favorable pathway because it relieves the ring strain from the cyclobutane while generating a tertiary alkyl radical with a new reactive double bond. In the presence of oxygen, O_2 combines with the alkyl radical to make a peroxy radical, which is then converted to an alkoxy radical via Reaction (R5) (denoted as R^5O here) (Atkinson and Arey, 2003a; Vereecken and Peeters, 2012). Reactions which can be accomplished by any of the radicals present (RO_2, HO_2, NO_3, etc) are symbolized by reaction with generic radical $\mathbf{L}^{\bullet}$, while hydrogen abstractions are symbolized by reaction with generic radical $\mathbf{Q}^{\bullet}$ (e.g., NO_3, RO_2, etc.). R^5O can undergo intramolecular addition to the less substituted C_7 of the newly formed double bond via Reaction (R6), generating a cyclic ether alkyl radical (Vereecken and Peeters, 2004, 2012). Alternatively, R^5O can undergo hydrogen abstraction from another species via Reaction (R7) to form a hydroxynitrate of MW = 215 amu (R^7OH), a gas-phase species detected by CIMS. The cyclic ether alkyl radical generated by Reaction (R6) combines with O_2 to make peroxy radical **U** by Reaction (R8). The fate of radical **U** is to produce a cyclic ether hydroxynitrate with MW = 231 amu via Reaction (R9) (Russell, 1957; Atkinson and Arey, 2003a). A compound with the same molecular weight as this species is detected by CIMS.

The alkyl radical formed in Reaction (R1) can also undergo a 1,5-CH_3 shift as indicated by Reaction (R3), which forms a tertiary alkyl radical that then combines with O_2 by Reaction (R10). Reaction (R10) produces a hydroxynitrate ($R^{10}OH$) with MW = 215 amu, an isomer that could also correspond to the species observed by CIMS. Further functionalization of $R^{10}OH$ continues after hydrogen abstraction by Reaction (R11), which bond strength calculations predict occur preferentially at the C_3 position (Vereecken and Peeters, 2012). The resulting secondary alkyl radical from Reaction (R11) reacts with O_2 to form peroxy radical **S** via Reaction (R12). The reaction $\mathbf{S} + \mathbf{L}^{\bullet}$ forms either a hydroxycarbonyl nitrate with MW = 229 amu by Reaction (R13), or a dihydroxynitrate with MW = 231 amu by Reaction (R14) (Russell, 1957; Atkinson and Arey, 2003a). Both are gas-phase species detected by CIMS.

The peroxy radical formed in Reaction (R2) can be converted to a hydroperoxide with MW = 231 amu (observed in CIMS) by reaction with an HO_2 radical (R15). Since Reaction (R15) is

only associated with the RO_2+HO_2 channel, the signal corresponding to the species with MW = 231 amu is expected be higher in the "RO_2+HO_2 dominant" experiments. Figure S2 shows the CIMS signal at m/z = 358 (MW = 231 amu) normalized to Br_2 sensitivity for each type of experiment ("RO_2+NO_3 dominant" and "RO_2+HO_2 dominant", dry and humid conditions). The higher signal in the "RO_2+HO_2 dominant" experiments supports the formation of more ROOH species in the gas phase under this reaction condition.

The peroxy radical formed from Reaction (R2) can also be converted into an alkoxy radical, $R^{16}O$, via Reaction (R16). Hydrogen abstraction by the alkoxy radical $R^{16}O$ can form a third hydroxynitrate isomer with MW = 215 amu by Reaction (R17). Alternatively, $R^{16}O$ can undergo a 1,5-H shift from a $–CH_3$ group by Reaction (R18) to form an alkyl radical at one of the terminal carbons (Carter et al., 1976; Eberhard et al., 1995; Atkinson, 1997; Dibble, 2001). The alkyl radical then reacts with O_2 to form a peroxy radical and subsequently forms an aldehyde with MW = 229 by the overall Reaction (R19) (Russell, 1957; Atkinson and Arey, 2003a). The aldehydic hydrogen is especially susceptible to undergoing hydrogen abstraction (Miller, 1999), followed by O_2 addition to form a peroxy acid radical, and final conversion to a carboxylic acid (Russell, 1957; Atkinson and Arey, 2003a). $R^{20}COOH$ with MW = 245 amu is produced by Reaction (R20), a species registered as an anion by UHPLC-MS at *m/z* 244 (MW = 245 amu) (Fig. S5). CIMS data also support the pathways via Reaction (R20) (Fig. 2). The Br_2-normalized CIMS signal for species at *m/z* 356 (MW = 229 amu) decreases with a subsequent increase in species at *m/z* 372 (MW = 245 amu) in the gas phase over the course of the experiment. Due to the lower vapor pressure of carboxylic acid species compared to carbonyl species (Pankow and Asher, 2008), the majority of carboxylic acid formed from this channel is expected to partition into the particle phase. In addition to Reaction (R20), $R^{20}COOH$ can also be formed through a more direct route by addition of O_2 to the alkyl radical product and then subsequent reaction of the peroxy radical with HO_2 via the sequence of Reactions (R18) + (R21) + (R22) (Ziemann and Atkinson, 2012).

The hydroxynitrate formed by Reaction (R17) can also undergo hydrogen abstraction at the C_3 position, as indicated by Reaction (R23). (Vereecken and Peeters, 2012). Reaction (R24) shows how O_2 addition to the resulting secondary alkyl radical gives peroxy radical **T**, which can either

react with **L**$^{\bullet}$ to form a dihydroxynitrate with MW = 231 amu via Reaction (R25) or form a hydroxycarbonyl nitrate with MW = 229 amu via Reaction (R26) (Russell, 1957; Atkinson and Arey, 2003a). In the absence of hydrogen atoms in the C_3 position, hydrogen abstraction occurs from C_4 of the hydroxycarbonyl nitrate species via Reaction (R27) (Vereecken and Peeters, 2012), which then forms a peroxy radical **V** by Reaction (R28) (Atkinson and Arey, 2003a). Reaction (R29), **V** + **L**$^{\bullet}$, yields a dihydroxycarbonyl nitrate with MW = 245 amu (Russell, 1957; Atkinson and Arey, 2003a). This dihydroxycarbonyl nitrate is not expected to be the species appearing in the UHPLC-MS chromatogram (Fig. S5) at *m/z* 244 (MW = 245 amu) because it lacks a –COOH group and likely has a higher vapor pressure than the carboxylic acid species with MW = 245 amu. Instead, it is likely that the dihydroxycarbonyl nitrate is the species observed by CIMS at *m/z* 372 (MW = 245 amu). A third possible isomer (not shown in Fig. 8) with MW = 245 amu and containing a non-carboxylic C=O group, could be similarly formed from the product of Reaction (R13). Likewise, other isomers to those generated after Reaction (R26) can be formed from each possible structure with MW = 229 amu, providing a wide array of precursors to form heavier MW products. The confirmation that several isomers with MW = 245 amu are present in the filter extracts is revealed from the extracted ion chromatogram, EIC, which shows closely eluting peaks at *m/z* 244 (MW = 245 amu) when substituting formic acid for acetic acid (Li et al., 2011) as the modifier in the mobile phase (Fig. S5).

4.2) Aerosol Yields

4.2.1) SOA Yields Over a Wide Range of Organic Mass Loadings

The SOA yields obtained from this study are shown in Fig. 3 and Fig. 4. In recent years, it has been suggested that the loss of organic vapors to the chamber wall could affect SOA yields (Matsunaga and Ziemann, 2010; Loza et al., 2010; Yeh and Ziemann, 2014; Zhang et al., 2014; Zhang et al., 2015). Specifically, Zhang et al. (2014) demonstrated that vapor wall loss could lead to an underestimation of SOA yields by as much as a factor of 4. To evaluate the potential effect of organic vapor wall loss on SOA yields in our study, experiments without seed are carried out at different conditions (dry and humid (RH = 50, 70%); "RO_2+NO_3 dominant" and "RO_2+HO_2 dominant" conditions). The yields from the nucleation experiments are reported in

Fig. S9 along with the yield curve obtained from seeded experiments. The similar yields for nucleation/seeded "RO_2+NO_3 dominant" experiments (dry and humid) in our study suggest that vapor wall loss has a negligible effect on aerosol yields in these experiments. It is likely that rapid reaction of β-pinene with nitrate radicals in this study mitigate the effect of organic vapor wall loss on SOA yields. Based on the rapid SOA growth (peak growth typically achieved within 10-15 minutes) for these experiments, it is estimated that the effective reaction rate of β-pinene in our experiments is an order of magnitude higher than the rates reported in Zhang et al. (2014). Although the aerosol mass yields for the "RO_2+HO_2 dominant" nucleation experiments are lower than the corresponding seeded experiments, further increase in the seed concentration does not have a significant effect on yield. Zhang et al. (2014) determined that if vapor phase wall loss is significant in chamber experiments, the addition of more seed particles will lead to an increase in SOA yield. Therefore, it is likely vapor phase wall loss is also negligible in our seeded "RO_2+HO_2 dominant" experiments. It is unclear at this time why nucleation experiments have lower SOA yield only for the "RO_2+HO_2 dominant" experiments. One possibility is that the chamber-wall uptake of ROOH species (which is likely higher in "RO_2+HO_2 dominant" experiments as measured by CIMS (Fig. 2)) is more rapid than other gas-phase species.

A comparison of aerosol yields obtained for the oxidation of β-pinene with nitrate radicals is also shown in Fig. 3. Griffin et al. (1999) performed the first comprehensive study of SOA formation from nitrate radical oxidation of BVOCs. The aerosol yield curve reported for β-pinene+NO_3 by Griffin et al. (1999) is shown next to our yield curve in Fig. 3. The yield curve in Griffin et al. (1999) was generated from chamber experiments with $\Delta M_o > 45$ μg m^{-3} (range of $\Delta M_o = 45–660$ μg m^{-3}) and extrapolated down to lower loadings. The yield curve generated in the current study, however, includes measurements at mass loadings < 10 μg m^{-3} and does not require any extrapolation beyond the bounds of the data to include lower, atmospherically relevant aerosol loadings. As shown in Fig. 3, while the SOA yields from this study are consistent with Griffin et al. (1999) for $\Delta M_o > 45$ μg m^{-3}, the yields from this study are as much as a factor of 4 higher than those reported by Griffin et al. (1999) at lower mass loadings.

Instances where the measured yields at low mass loading do not match those extrapolated from higher loadings have been observed for α-pinene ozonolysis (Presto and Donahue, 2006). We

attribute this result to limitations of the two-product model, which bins all compounds into only two semi-volatile products of differing vapor pressures, to cover the entire spectrum of volatilities for all chemical products. At higher mass loadings, semi-volatile and volatile compounds can condense onto the particle phase and can potentially make up the majority of the aerosol. When a two-product yield curve is fit to high mass loadings only, the parameters are likely to be biased by the semi-volatile and high volatility products. Therefore, a yield curve fit using data from only high mass loadings will not account for the low-volatility products, which might be the minority products at high organic mass loadings. The two-product fit using high mass loadings therefore cannot be used to predict yields at low mass loadings, where the SOA is mostly comprised of low-volatility products. Since the yield curve generated as part of this study spans a wide range of organic mass loadings, the fitting parameters account for both the low-volatility products and the higher volatility products.

Fitting yield data to the volatility basis set described in Donahue et al. (2006) illustrates how higher volatility bins (products) are favored at higher aerosol mass loadings. The fit coefficients for the volatility basis set are shown in Table 3 for the aerosol yields of β-pinene+NO_3 from this study and that of Griffin et al. (1999). It is noted that the data from Griffin et al. (1999) have been adjusted to a temperature of 298 K and density of 1.41 g cm^{-3} for comparison to results from our study. As seen in Table 3, the stoichiometric coefficients for the fit of Griffin et al. (1999) are weighted towards higher volatility products while the coefficients fit to the data collected in this study are distributed among lower and higher volatility products.

Fry et al. (2009) conducted a pair of β-pinene+NO_3 chamber experiments under dry and humid (RH = 60%) conditions. Their results are also shown in Fig. 3. The yields from Fry et al. (2009) are about 20% lower than the current study. A more recent study by Fry et al. (2014) reported aerosol mass yields in the range of 33-44% for the β-pinene+NO_3 system at an organic mass loading of 10 μg m^{-3} in a continuous flow chamber under dry conditions. This is approximately 10-30% lower than the yield reported at a similar mass loading in this study. While various experimental conditions can contribute to the difference in aerosol mass yields, we note that the aerosol formation rate in both Fry et al. (2009) and Fry et al. (2014) is slower than this study, which is likely caused by lower oxidant concentrations in Fry et al. (2009) and Fry et al. (2014)

611 compared to this study. Slower reaction times could allow more time for the gas-phase species to
612 partition onto the chamber walls and reduce the amount that partitions onto aerosol (Ng et al.,
613 2007a; Zhang et al., 2014). Thus, organic vapor wall loss might play a role in the lower yields
614 observed in Fry et al. (2009) and Fry et al. (2014). There is a substantial difference between our
615 β-pinene+NO_3 SOA yield and that from Hallquist et al. (1999), which reported an aerosol mass
616 yield of 10% for a mass loading of 4 μg m^{-3}. A possible explanation for this is that the mass of β-
617 pinene reacted was not directly measured in Hallquist et al. (1999), instead, it was assumed that
618 the concentration of β-pinene reacted was equivalent to the concentration of N_2O_5 reacted. If
619 there were other loss processes for N_2O_5 in the experiments conducted by Hallquist et al. (1999),
620 the yield reported in their study could be substantially lower than the actual aerosol yield.
621

622 **4.2.2) Effects of RH and Acidity on SOA Yields**

623

624 For the "RO_2+NO_3 dominant" experiments, the yields between experiments conducted at dry
625 conditions with ammonium sulfate seed are similar to experiments conducted under high
626 humidity (RH = 50% and RH = 70%) (Fig. 3). Our results indicate that the relative humidity
627 does not have appreciable effects on the aerosol mass yield. These results are consistent with
628 previous humidity effects studies on photooxidation (Nguyen et al., 2011) and nitrate radical
629 chemistry (Bonn and Moorgat, 2002; Fry et al., 2009). However, these results are inconsistent to
630 the study performed by Spittler et al. (2006), where lower SOA yields were obtained for the α-
631 pinene+NO_3 system under humid conditions (RH = 20%). Spittler et al. (2006) proposed that
632 either the presence of water vapor altered the gas-phase chemistry or that the aerosol water on
633 seed particles prevented gas-phase partitioning. These do not seem to be the case in our study.
634 Similar gas-phase oxidation products are detected by CIMS under both dry and humid conditions
635 and the organics size distribution measured by HR-ToF-AMS overlaps that of the seed aerosol,
636 indicating that the oxidation products are condensing onto the seed particles.
637

638 The presence of aerosol water can potentially affect SOA formation through hydrolysis of
639 organic nitrates. It has been observed in previous studies that organic nitrates in aqueous filter
640 extract can undergo hydrolysis to form alcohols and nitric acid (Sato, 2008). The change from
641 nitrate to hydroxyl functional groups could affect gas-particle partitioning and aerosol yields if

642 the organic nitrates and alcohols have different vapor pressures. However, previous studies have
643 shown that hydroxyl groups lower the vapor pressure of an organic compound to the same extent
644 as organic nitrate groups (Pankow and Asher, 2008). In this study, hydrolysis does not appear to
645 be a major reaction pathway for β-pinene+NO_3 SOA under humid conditions. As shown in
646 Section 4.4, only < 10% of OA undergoes hydrolysis. Thus, even if there is a difference in the
647 vapor pressures between organic nitrates and their hydrolysis products, it is unlikely that this
648 would affect aerosol yields in our case.
649
650 Aerosol water can also enhance SOA yields by providing a medium for water-soluble species
651 (e.g., glyoxal) to dissolve into the particulate aqueous phase (Ervens et al., 2011). Nitrate radical
652 addition is predicted to add predominantly to a double bond instead of cleaving carbon to carbon
653 bonds (Wayne et al., 1991) and hence fragmentation to small carbon compounds is unlikely. As
654 shown in Fig. 8, the proposed mechanism does not involve carbon cleaving reactions which
655 could result in small, water-soluble compounds. This is further supported by the similarities in
656 SOA yields between dry and humid conditions. If these carbon cleaving reactions dominate and
657 form small, water-soluble species, the yields should be much higher for the humid conditions
658 than the dry conditions.
659
660 We find that aerosol acidity has a negligible effect on the SOA yield for the β-pinene+NO_3
661 system (Fig. S4). This is opposite to some previous studies where increases in aerosol yields
662 have been found under acidic conditions for other SOA systems (using the same seeds as in our
663 study), such as ozonolysis of α-pinene and photooxidation of isoprene (e.g., Gao et al., 2004;
664 Surratt et al., 2007). Acid-catalyzed particle-phase reaction such as oligomerization has been
665 proposed for such "acid effects". Although aerosol produced by the β-pinene+NO_3 reaction can
666 potentially undergo oligomerization as well, it appears that the aerosol products are of low
667 enough volatility that further particle-phase reactions (if any) do not enhance SOA yields. This
668 indicates that the "acid effect" is likely different for different SOA systems, which would depend
669 on the parent hydrocarbon, oxidant (ozone, OH, nitrate radicals), and other reaction conditions.
670 In general, the SOA yields for nitrate radical oxidation of BVOCs are higher than corresponding
671 yields in ozonolysis or OH radical oxidation (e.g., Griffin et al., 1999), suggesting that no further

particle-phase reaction is needed to make the oxidation products more non-volatile and the "acid effect" could be limited.

4.2.3) Effects of RO_2+NO_3 vs. RO_2+HO_2 Chemistry on SOA Yields

Previous studies have shown that the fate of peroxy radicals can have a substantial effect on SOA formation (Kroll and Seinfeld, 2008; Ziemann and Atkinson, 2012). For instance, it has been shown in laboratory chamber studies that the aerosol yields can differ by a factor of 2 depending on the RO_2 fate for the isoprene+NO_3 system (Ng et al., 2008). Although studies have proposed that RO_2+NO_3 is the major nighttime RO_2 fate in the ambient environments (Kirchner and Stockwell, 1996), results from recent field studies suggested that HO_2 radicals are abundant at night (Mao et al., 2012). The high HO_2 radical concentration could result in the RO_2+HO_2 reaction becoming the dominant RO_2 radical fate in the nighttime atmosphere. In our study, the experimental protocols are designed to promote the "RO_2+NO_3" or "RO_2+HO_2" reaction channel. These two scenarios would be representative of nitrate radical oxidation in environments with varying levels of NO_x. To our knowledge, this is the first study in which the fate of peroxy radicals is considered in SOA formation from nitrate radical oxidation of monoterpenes. A simple kinetic model based on MCMv3.2 (Saunders et al., 2003) is developed to simulate the gas-phase chemistry for the β-pinene+NO_3 reaction. The simulation results suggest that in both "RO_2+NO_3 dominant" and "RO_2+HO_2 dominant" experiments, the cross-reactions of RO_2 radicals are not a significant reaction pathway (Fig. S10). Figure 4 shows that the SOA yields from the "RO_2+HO_2 dominant" experiments are similar to the "RO_2+NO_3 dominant" experiments. The similar yields under these different reaction conditions could arise from a comparable suite of reaction products between the two reaction pathways. The reaction of RO_2+NO_3 produces an RO radical (Fig. 8, Reaction R16) which can undergo decomposition or isomerization (Orlando and Tyndall, 2012; Ziemann and Atkinson, 2012). Typically, it is expected that the RO_2+HO_2 reaction will lead to the formation of peroxides (Orlando and Tyndall, 2012; Ziemann and Atkinson, 2012). However, a recent study by Hasson et al. (2012) showed that for highly substituted peroxy radicals, the RO_2+HO_2 reaction favors the formation of RO radicals. Additionally, several previous studies showed that as carbon chain length increases (C2-C4), the RO_2+HO_2 reaction becomes less likely to form the ROOH product and more likely

to form the RO product (Jenkin et al., 2007; Dillon and Crowley, 2008; Hasson et al., 2012). In the case of β-pinene+NO_3, RO_2 radicals are expected to form on the tertiary carbon as the nitrate radicals tend to attack the least substituted carbon of a double bond, leading to the formation of tertiary peroxy radicals (Wayne et al., 1991) (Fig. 8). Given β-pinene is a C10 compound and forms a highly substituted peroxy radical, we hypothesize that the RO_2+HO_2 reaction pathway in our study forms RO radicals as suggested by Hasson et al. (2012), leading to a similar peroxy radical fate as in the "RO_2+NO_3 dominant" experiments. We note that the RO_2+HO_2 reaction still leads to formation of ROOH as measured by CIMS (Fig. S2). Thus it appears that the RO_2+HO_2 channel does not exclusively produce RO radicals in our case. Nevertheless, based on the similar SOA yields in the " RO_2+NO_3 dominant" and "RO_2+HO_2 dominant" experiments, we propose that either the RO radical is the dominant product of the RO_2+HO_2 reaction pathway, or that ROOH has a similar volatility to the products formed from the RO radicals in the "RO_2+NO_3 dominant" experiments.

SOA is collected on filters for several experiments and analyzed using UHPLC in order to characterize the particle composition. Figure 9 shows the ratios of the total areas under the UV-visible chromatograms for "RO_2+HO_2 dominant" and "RO_2+NO_3 dominant" experiments, under both humid and dry conditions. Chromatograms collected at 205, 235, and 270 nm are integrated to get the total area at each wavelength and the standard deviation from two measurements. Total areas are normalized by the estimated organic mass loading on the corresponding filters. The wavelengths chosen represent a good proxy for certain functional groups that absorb in these regions. More specifically, λ = 235 nm corresponds to a region of strong absorption by ROOR and ROOH (Farmer et al., 1943; Turrà et al., 2010; Ouchi et al., 2013), while λ = 270 nm is a compromise wavelength that represents both carbonyl and alkyl nitrate functional groups (Xu et al., 1993; Pavia et al., 2008). Finally, λ = 205 nm is chosen as the normalization wavelength because practically all organic matter present in the sample absorbs in this UV region. Figure 9 shows the ratio of total areas at 235 nm and 270 nm relative to the value at 205 nm, which provides a qualitative comparison of the samples. By comparing the amounts (areas) of the 235 and 270 nm absorbing species, the effect of humidity on each branching pathway (RO_2+HO_2 or RO_2+NO_3) can be assessed. How much -ONO_2, -C=O, ROOR and ROOH is produced under each humidity level determines the relative reactivity between the humid vs. dry conditions of

each branching pathway. The relative reactivity for both reaction channels is similar within one standard deviation for all humidity conditions studied, indicating that each condition may have a similar product distribution. A comparison between the RO_2 + HO_2 and RO_2 + NO_3 pathways cannot be made in this manner because NO_3 concentrations are different. The seemingly smaller areas for species produced in the HO_2 panel could simply be due to a larger amount of non-nitrated organic matter being produced that absorbs at the normalization wavelength. However, one slight difference is the enhancement in the production of $C_{10}H_{15}NO_6$ (*m/z* 244, an RCOOH species) in the "RO_2+HO_2 dominant" experiments, which increases by 2 and 7 times under dry and humid conditions, respectively, relative to the "RO_2+NO_3 dominant" experiments. This observation indicates that in the presence of additional HO_2, the oxidation is directed toward the synthesis of $C_{10}H_{15}NO_6$ (*m/z* 244) more efficiently. This can be explained by an enhancement of the reaction sequence R21 + R22 in Fig. 8, which is enhanced at high HO_2 radical concentrations.

4.3) Particulate Organic Nitrate Formation and Hydrolysis

4.3.1) Organic Nitrate Formation

The mass spectrum in Fig. 5 indicates the presence of a large fraction (11%) of nitrate in the aerosol formed from the β-pinene+NO_3 reaction. Approximately 90% of the N atoms in the spectrum are found on the NO^+ and NO_2^+ fragments. Most of the nitrate signal is assumed to be from organic species (i.e., organic nitrates) as N_2O_5 uptake to the particles is negligible and the NO^+:NO_2^+ ratio is high. In humid experiments, the heterogeneous hydrolysis of N_2O_5 could lead to the formation of inorganic nitrates (e.g., HNO_3). To evaluate the contribution of inorganic nitrates to the total NO^+ and NO_2^+ ions measured by the HR-ToF-AMS, we perform two characterization experiments (RH = 50%) in which only N_2O_5 (the maximum amount of N_2O_5 used in our aerosol experiments) and seed aerosol ($(NH_4)_2SO_4$ seed or $(NH_4)_2SO_4$+H_2SO_4 seed) are injected into the chambers. In both cases, using a relative ionization efficiency (RIE) of 1.1 for nitrate results in a nitrate growth of less than 0.1 μg m^{-3} detected by the HR-ToF-AMS (Rollins et al., 2009). The uptake of N_2O_5 is even less likely in the SOA yield experiments. It has been shown that when comparing to inorganic seed only, the presence of organic matter

decreased N_2O_5 uptake by 80% (Gaston et al., 2014). Therefore, the contribution of inorganic nitrates to the total nitrate signals measured by the HR-ToF-AMS in our experiments is negligible.

It has been shown previously that the NO^+:NO_2^+ ratio in the HR-ToF-AMS mass spectrum can be used to infer the presence of particle-phase organic nitrates (Farmer et al., 2010). Specifically, Farmer et al. (2010) suggested that the NO^+:NO_2^+ ratio is much higher for organic nitrates (ratio = 5-15) than inorganic nitrates (ratio ~2.7) and therefore, aerosol with a high NO^+:NO_2^+ ratio likely also has a high concentration of organic nitrates. Figure 5 shows that approximately only two-thirds of the signal at *m/z* 30 is from NO^+, while the remaining signal is from organic CH_2O^+ fragment. At peak aerosol growth under dry and humid conditions, we determine from the high-resolution AMS data that the average R-ON value for β-pinene+NO_3 aerosol is 6.5 in "RO_2+NO_3 dominant" experiments and an average of 8.6 in "RO_2+HO_2 dominant" experiments. Previous studies (Fry et al., 2009; Bruns et al., 2010) on the β-pinene+NO_3 reaction suggested that the R-ON for β-pinene+NO_3 SOA is on the order of 10:1, higher that the values determined in this study. One possible explanation for the difference in R-ON between this study and previous literature is instrument bias. Different instruments may have different R-ON values. One way to circumvent this bias is to compare the R-ON:R-AN ratio. The R-ON:R-AN for all experiments is 3.9, which is in agreement with values calculated by Fry et al. (2009) and Bruns et al. (2010) (range 3.7-4.2).Another explanation for this difference is the close proximity of the CH_2O^+ ion to the NO^+ ion in the aerosol mass spectrum, which may result in a small bias in the calculated R-ON. Specifically, if we were to include the contribution of the organic CH_2O^+ and $CH_2O_2^+$ fragments at *m/z* 30 and *m/z* 46 (in addition to contribution from NO^+ and NO_2^+), respectively, the corresponding NO^+:NO_2^+ ratios would be higher, i.e., 9:1 for "RO_2+NO_3 dominant" experiments and 11:1 for "RO_2+HO_2 dominant" experiments. Therefore, when using the NO^+:NO_2^+ ratio to estimate organic nitrate contribution in ambient OA, it is imperative that one excludes the organic contribution (if any) at *m/z* 30 when calculating the ratio.

One possible way to estimate the molar fraction of organic nitrates in the aerosol from the HR-ToF-AMS data is to use the N:C ratio of the aerosol formed in the experiments. Since β-pinene is a monoterpene, we assume its oxidation products have approximately 10 carbon atoms. This is a

reasonable assumption based on the gas-phase oxidation products detected by CIMS (Fig. 8). The dominant reaction pathway of nitrate radicals is addition via attack of the double bond, adding one nitrate group to the primary carbon and forming a peroxy radical. With one nitrate group and 10 carbons from the β-pinene precursor, the organic nitrate products are expected to have a N:C ratio of about 1:10. If 100% of the SOA formed is composed of organic nitrates, the HR-ToF-AMS data should have a N:C ratio of 0.1. The average N:C ratio for all experiments measured by the HR-ToF-AMS is approximately 0.074 for SOA formed from β-pinene+NO_3 at peak growth. Thus, as an upper bound, it is approximated that the molar fraction of organic nitrates in the aerosol is 74%. Even if there is fragmentation, the organic nitrate fraction in the aerosol would remain fairly high. For instance, if the organic nitrate species only has 9 carbons, the upper-bound molar organic nitrate fraction is approximately 67%. If we assume the organic nitrate and non-organic nitrate species have the same molecular weight, the molar organic nitrate fraction in the aerosol is equal to the fraction of aerosol mass composed of organic nitrates. In addition to N:C, the HR-ToF-AMS Nitrate:Org mass ratio can also be used to estimate the particle organic nitrate fraction. The average Nitrate:Org mass ratio measured by the HR-ToF-AMS for all experiments is about 0.16. We assume the organic nitrate compound has an average molecular weight between 200 and 300 amu based on the predicted products (Fig. 8), where 62 amu is attributed to the nitrate group while the remaining mass is from the organic mass. Using both the Nitrate:Org mass ratio and the assumed range of molecular weights for the organic nitrate species, the fraction of aerosol mass composed of organic nitrates is estimated to be 45-68%. We estimate that the fraction of aerosol mass composed of organic nitrates is 60%, based on the average value of the extremes of the two estimates. This is comparable to the fraction of aerosol mass composed of organic nitrates estimated by Fry et al. (2014) (56%) but higher than that reported by Fry et al. (2009) (30-40%). The different experimental conditions in our study vs. those in Fry et al. (2009) may have contributed to the difference in the fraction of aerosol mass composed of organic nitrates. For example, the ratio of NO_2 to O_3 used to make NO_3 radicals in Fry et al. (2009) is lower than this study, which may have led to differing branching ratios of β-pinene+NO_3 vs. β-pinene+O_3.

827 **4.3.2) Hydrolysis and Organic Nitrate Fate**

828

829 As shown in Fig. 7, for experiments with the same initial hydrocarbon concentration, the AMS
830 nitrate-to-organics ratio of the humid experiments normalized by the dry experiments stabilize at
831 a ratio of about 0.9. The nitrate radical addition at the double bond of β-pinene can lead to the
832 formation of either primary or tertiary nitrates. Previous studies of organic nitrate hydrolysis in
833 bulk solutions showed that while saturated primary nitrates hydrolyze on the order of months,
834 tertiary nitrates hydrolyze on the order of hours (Darer et al., 2011). Primary organic nitrates with
835 double bonds can hydrolyze on the order of minutes (Jacobs et al., 2014), but oxidation products
836 from the β-pinene+NO_3 reaction are likely saturated compounds due to the lone double bond of
837 β-pinene (Fig. 8). Therefore, the point at which nitrate mass stops decreasing is interpreted as
838 when all tertiary nitrates have hydrolyzed. As the oxidation products typically contain only one
839 nitrate group (Fig. 8), we infer that, within experimental error, approximately 90% of the organic
840 nitrates formed from the β-pinene+NO_3 reaction are primary nitrates. These results are consistent
841 with findings that nitrate radical is more likely to attack the less substituted carbon, which, in the
842 case for β-pinene, is the terminal carbon (Wayne et al., 1991). Since the nitrate addition is the
843 first reaction step, any subsequent differences in peroxy radical fate (e.g., RO_2+NO_3 vs.
844 RO_2+HO_2) will not affect the relative amount of primary vs. tertiary nitrates in our systems.

845

846 Based on the decay rate of $(Nitrate:Org)_{norm}$, the hydrolysis lifetime of the tertiary nitrates
847 formed in the reaction of β-pinene with nitrate radicals is calculated to be approximately 3-4.5
848 hr. This is on the same order of magnitude as the hydrolysis lifetime (6 hr) of the proposed
849 tertiary organic nitrates formed from photooxidation of trimethyl benzene in the presence of NO_x
850 (Liu et al., 2012). Results from our study therefore do not suggest that nitrate radical chemistry
851 produces organic nitrates with different hydrolysis rates than what is previously known for
852 primary or tertiary organic nitrates. Instead, this study proposes that the fraction of tertiary
853 organic nitrates produced from nitrate radical chemistry is much lower than SOA produced from
854 photooxidation in the presence of NO_x. While we directly demonstrate this to be true in the case
855 of the β-pinene+NO_3 system, this can also be applied to commonly emitted terpenes, including
856 those with internal double bonds. From the list of terpenes in Guenther et al. (2012), all
857 unsaturated terpenes have at least one double bond with a secondary or primary carbon. For

example, α-pinene contains an internal double bond connecting a tertiary carbon to a secondary carbon. The nitrate radical is more likely to attack the less substituted carbon (i.e. the secondary carbon) and form a secondary organic nitrate. As primary/secondary and tertiary organic nitrates have drastically different hydrolysis rates, it is imperative that their relative contribution be accurately represented in models when determining the fate of ambient organic nitrates. A recent study by Browne et al. (2013) modeled the hydrolysis of organic nitrates in a forested region by assuming that 75% of atmospheric organic nitrates formed in the day are composed of tertiary organic nitrates, based on the average fraction of tertiary organic nitrates from the photooxidation of α-pinene and β-pinene in the presence of NO_x. This has implications on not only the organic nitrate fate, but also on the formation of nitric acid, a byproduct of organic nitrate hydrolysis (Sato, 2008). With this, Browne et al. (2013) predicted that hydrolysis of organic nitrates produced in the day time could account for as much as a third to half of all nitric acid production. However, when considering organic nitrates formed both in the day and at night, the fraction of tertiary organic nitrates in ambient organic nitrates is likely lower than that used by Browne et al. (2013). This is especially true in areas where nitrate radical oxidation is the dominant source of organic nitrates (e.g., NO_x > 75 ppt in forested regions as noted in Browne et al. (2014)). It is recommended that future modeling studies of organic nitrates fates should consider organic nitrates formed both in the day and at night in order to take into account the large contribution of primary organic nitrates (which do not hydrolyze appreciably) formed from nitrate radical oxidation of monoterpenes.

Previous studies suggested that hydrolysis of organic nitrates can be an acid-catalyzed process in both solution (Szmigielski et al., 2010) and directly in the particle phase (Rindelaub et al., 2015). However, it has been found that primary and secondary organic nitrates are stable unless the aerosol is very acidic (pH < 0) (Darer et al., 2011; Hu et al., 2011). We calculate the corresponding change in $(\text{Nitrate:Org})_{norm}$ ratio for the experiments where $(NH_4)_2SO_4$+H_2SO_4 seed is used (data not shown in Fig. 7). We find that for these experiments, the $(\text{Nitrate:Org})_{norm}$ ratio also becomes constant at around 0.9, similar to that of the $(NH_4)_2SO_4$ seed experiments. However, the experiments using $(NH_4)_2SO_4$+H_2SO_4 seed have a more rapid rate of decrease in the $(\text{Nitrate:Org})_{norm}$ ratio. This suggests that while hydrolysis of tertiary nitrates is accelerated under more acidic conditions, primary organic nitrates do not hydrolyze at an observable rate for

the pH conditions employed in this study. As the majority of the particulate organic nitrates formed in our experiments are primary nitrates, we infer that particle acidity may not have a significant impact on the hydrolysis of organic nitrates formed in the BVOCs+NO_3 reaction, except in the cases where the double bond on the BVOCs connects two tertiary carbons, such as terpinolene.

4.4) Aerosol Aging in the Dark

While the aging of SOA has been extensively investigated in multiple photooxidation studies and shown to affect aerosol mass (e.g., Donahue et al., 2012; Henry and Donahue, 2012), little is known regarding aerosol aging by nitrate radicals (Qi et al., 2012). A number of theoretical (Kerdouci et al., 2010, 2014; Rayez et al., 2014) and experimental studies (Atkinson, 1991; Wayne et al., 1991) suggested that hydrogen abstraction by nitrate radicals occurs, especially for hydrogen atoms attached to aldehyde groups. As shown in Fig. 8, the β-pinene+NO_3 reaction can lead to the formation of compounds with carbonyl groups, allowing for potential nighttime aging of SOA by nitrate radicals. We focus our aerosol aging discussion on the "RO_2+NO_3 dominant" experiments, where the oxidant (nitrate radicals) concentrations are higher.

As aerosol ages, first-generation products either functionalize, which decreases volatility, or fragment, which can lead to an overall increase in volatility (Kroll et al., 2009). If fragmentation is the dominant pathway, a decrease in organic mass is expected as products become more volatile and re-partition back to the gas phase. We use the AMS Org:Sulfate ratio as a proxy to examine the effect of aerosol aging on organics mass in our experiments. As wall loss of particles will lead to a decrease in organic loading, normalizing the organic loadings by sulfate allows us to examine the net change in the organics mass over the course of the experiments. The use of Org:sulfate is a good proxy for aerosol aging when the organics only condense onto existing ammonium sulfate particles. A study by (Loza et al., 2012) has demonstrated that in the case of rapid condensation of organic species, the time scale of condensation is less than the time scale of diffusion to existing seed particle. When in this "diffusion-limited growth" regime, the organic mass partially nucleates to form new particles. Since the nucleated particles are smaller than those particles in which ammonium sulfate acted as a seed for condensation, organics

contained in these nucleated particles will be lost to the chamber walls more rapidly than the existing seed particles (Fig. S3). This could lead to an overall decrease in the Org:sulfate ratio. In our study, the Org:Sulfate ratio decreases after SOA reaches peak growth (Fig. 6). It is possible that this decrease is caused by wall loss of organic particles formed in the diffusion-limited growth regime. It is also possible that fragmentation of aerosol components is the dominant aging pathway, resulting in a decrease in the Org:Sulfate ratio. . Regardless, there is still evidence of increased functionalization over the course of the experiments. Rapid loss of organics due to particle wall loss or fragmentation of SOA would cause all AMS organic families to either decrease or remain constant relative to sulfate. However, Fig. 6 shows that the highly-oxidized fragments (CHOgt1, fragments with greater than 1 oxygen atom) increase slightly relative to sulfate while the non-oxidized fragments (CH) are lost at nearly twice the rate as the slightly oxidized fragments (CHO1). Since non-oxidized fragments are lost more quickly than less-oxidized fragments, it is possible that further particle-phase reactions are leading to the formation of highly oxidized compounds.

For the β-pinene+NO_3 reaction, carboxylic acids can be formed from the abstraction of hydrogen from aldehydes and subsequent oxidation (Fig. 8). The observed ions at *m/z* 356 and *m/z* 372 in CIMS likely correspond to hydroxy carbonyl nitrate and carboxylic acid, respectively. As shown in Fig. 2, *m/z* 356 decreases over the course of the experiment while *m/z* 372 increases. The possible conversion of aldehydes to carboxylic acids is also noticeable in the aerosol chemical composition. The *m/z* 44 (CO_2^+) fragment in the HR-ToF-AMS data likely arise from thermal-decomposition of carboxylic acids (Duplissy et al., 2011) and is commonly used to infer the extent of aerosol aging (Ng et al., 2011). Although the f_{44} (fraction of CO_2^+ ion to total organics) in the typical mass spectrum of β-pinene+NO_3 SOA is low (< 3%), there is a noticeable and continued increase in f_{44} after peak aerosol growth (Fig. 6). Specifically, during the 2.5 hours following peak growth, f_{44} increases by as much as 30% under dry conditions. Under humid conditions, the increase in f_{44} is only 6%. These correspond to a 17% and 6% increase in O:C ratio of the aerosol under dry (O:C ranging from 0.46 to 0.54 for all experiments) and humid conditions (O:C ranging from 0.47 to 0.50), respectively. The lower degree of aging in humid experiments is consistent with the observation that the CIMS N_2O_5 signals, while not quantified, are clearly lower (by at least a factor of 2) in the humid "RO_2+NO_3 dominant" experiments when

compared to dry experiments. This is likely due to the uptake of N_2O_5 to wet chamber and/or aerosol surfaces (Thornton et al., 2003).

It is unlikely that the observed decrease in organic species relative to sulfate and the decrease in gas phase species are due to differences in vapor phase wall loss. Matsunaga and Ziemann (2010) determined that highly-oxidized gaseous organic compounds are lost to the chamber walls faster than compounds that have a lower degree of oxidation. Additionally, the gas-wall partitioning coefficient for a specific compound has also been shown to increase with decreasing vapor pressure (Yeh and Ziemann, 2014), with highly oxidized species typically having lower vapor pressures than less oxidized species (Pankow and Asher, 2008). If vapor-phase wall loss is the driving factor for the decrease of organics in this study, it would be expected that oxidized compounds would be lost to the walls more rapidly. Subsequently, these highly oxidized compounds would re-partition back to the gas phase in order to re-establish particle-gas equilibrium. The decrease in organics shown in Fig. 6, however, indicates more rapid losses of non-oxidized fragments compared to oxidized fragments. The less oxidized species measured by CIMS (lower molecular weight) as shown in Fig. 2 also decrease more rapidly than the more oxidized species. Therefore, the change in chemical composition and decrease in vapor phase species is more likely attributable to aerosol aging than to vapor-wall partitioning.

5) Relevance to Ambient Measurements

Results from this study provide the fundamental information to evaluate the extent to which nitrate radical oxidation of monoterpenes contributes to ambient organic aerosol. This reaction provides a direct mechanism for linking anthropogenic and biogenic emissions, and is likely substantial in the southeastern United States, where both types of emissions are high. A recent field campaign, the Southeastern Oxidant and Aerosol Study (SOAS), took place in Centreville, Alabama from June 1st – July 15th, 2013 to investigate the effects of anthropogenic pollution in a region with large natural emissions. Based on positive matrix factorization (PMF) analysis of the HR-ToF-AMS data obtained in SOAS, Xu et al. (2015b) identified an OA subtype termed as less-oxidized oxygenated organic aerosol (LO-OOA), which accounted for 32% of the total OA at Centreville. LO-OOA peaks at night and is well-correlated with particle-phase organic

nitrates. These suggest that LO-OOA is produced predominantly from nighttime monoterpene+NO_3 chemistry, especially from β-pinene+NO_3 as β-pinene has a high nighttime concentration (Xu et al., 2015b). Results from the current laboratory chamber study provide the relevant fundamental data for estimating the amount of aerosol produced from monoterpene+NO_3 in SOAS. The campaign-average loading of non-refractory PM_1 in SOAS is about 8 μg m^{-3} and it has been determined that the aerosol is highly acidic (pH = 0.94±0.59) and contains a large amount of particulate water (5.09±3.76 μg m^{-3}) (Cerully et al., 2014; Guo et al., 2015). At night, the RH can reach up to 90% during the SOAS measuring period (Guo et al., 2015). The current chamber study is designed to probe SOA formation from nitrate radical oxidation under atmospherically relevant loadings, under high humidity, and in the presence of seed aerosol of different acidity. The fates of peroxy radicals at night are highly uncertain, which mainly arises from the lack of constraints on the reaction rates of the peroxy radicals with other species, such as RO_2+NO_3 (Brown and Stutz, 2012). In our study, the experiments are conducted under both "RO_2+NO_3 dominant" and "RO_2+HO_2 dominant" regimes to explore the effects of peroxy radial fates on SOA formation. Using a SOA yield of 50% (for a mass loading of 8 μg m^{-3} obtained from the yield curve) in the presence of acidic seed at RH = 70% obtained from "RO_2+HO_2 dominant" experiments, Xu et al. (2015b) estimated that about 50% of nighttime OA production could be due to the reaction of β-pinene with nitrate radicals in SOAS.

It is noted that the LO-OOA factor is also resolved at both rural and urban sites around the greater Atlanta area in all seasons, where HR-ToF-AMS measurements were conducted as part of the Southeastern Center for Air Pollution and Epidemiology study (SCAPE) (Verma et al., 2014; Xu et al., 2015a, b). It is found that LO-OOA made up 18-36% of the total OA in rural and urban areas, suggesting that a fairly large fraction of total OA in the southeastern United States could arise from nitrate radical oxidation of monoterpenes.

Figure 10 shows a comparison of the aerosol mass spectrum from a typical β-pinene+NO_3 experiment from this study and the LO-OOA factor obtained from SOAS data. As LO-OOA could have other sources in addition to monoterpene+NO_3, the two spectra are not in perfect agreement but they do show similar trends above *m/z* 60. Most noticeable of these are *m/z* 67 ($C_5H_7^+$) and *m/z* 91 ($C_7H_7^+$) with a ratio of these two ions ($C_5H_7^+$: $C_7H_7^+$) of about 2.9 (ranging

from 2.5-3.6 in other experiments). The mass spectra for the other SOA-forming systems predicted to be of importance at SOAS, namely, α-pinene ozonolysis (Chhabra et al., 2010), isoprene photooxidation (Chhabra et al., 2010), and nitrate radical initiated isoprene chemistry (Ng et al., 2008), do not show significant intensities at either of these two ions. Therefore, it is likely that high signals at $C_5H_7^+$ and $C_7H_7^+$ in ambient aerosol mass spectrum could be indicative of the presence of β-pinene+NO_3 reaction products. We note that the average NO^+:NO_2^+ ratio for aerosol measured at SOAS is 7.1, consistent with the high NO^+:NO_2^+ ratio from the SOA formed from nitrate radical oxidation of β-pinene in this study.

The gas-phase oxidation products detected by the CIMS in this study can also be used to help interpret ambient data to evaluate the possible contribution of β-pinene+NO_3 reaction. For instance, a significant amount of gas-phase organic nitrate species with MW of 215 amu and 231 amu have been observed during the BEARPEX campaign in Fall 2009 (Beaver et al., 2012). As these species exhibited a nighttime peak, Beaver et al. (2012) suggested that they could arise from nighttime oxidation of α-pinene or β-pinene by nitrate radicals. The proposed mechanism for β-pinene+NO_3 (Fig. 8) show multiple reaction pathways to form species with MW = 215 and MW = 231. Therefore, the oxidation of β-pinene by nitrate radicals represents one possible pathway for the formation of the species detected by Beaver et al. (2012). As the β-pinene+NO_3 reaction has shown to be important at SOAS (Xu et al., 2015b), it is expected that the gas-phase compounds observed in this chamber study could help explain some of the species detected by the multiple CIMS deployed during the SOAS study.

6) Atmospheric Implications

Although photooxidation is expected to be the major oxidation pathway for atmospheric VOCs, nitrate radical oxidation can account for as much as 20% of global BVOCs oxidation and is predicted to lead to an aerosol mass increase by as much as 45% when compared to the modeled case where this chemistry is excluded (Pye et al., 2010). Due to high SOA yields, evaluating the mass of aerosol produced by nitrate radical initiated chemistry is essential to estimate the total organic aerosol burden, both on regional and global scales. Currently, the aerosol yields from nitrate radical oxidation of monoterpenes in most models are assumed to be the same as those

determined from β-pinene+NO_3 reactions in Griffin et al. (1999) (Pye et al., 2010). In this study, we systematically investigate SOA formation from the nitrate radical oxidation of β-pinene under various reaction conditions (dry, humid, differing radical fate) and a wide range of initial hydrocarbon concentrations that are atmospherically relevant. We determine that the SOA yields from the β-pinene+NO_3 systems are consistent with Griffin et al. (1999) for mass loadings > 45 μg m^{-3}, but as much as a factor of 4 higher than those reported in Griffin et al. (1999) for lower mass loadings. The lower SOA yields reported in Griffin et al. (1999) could arise from uncertainties in extrapolating data from higher mass loadings to lower mass loadings in that study, as well from slower reaction rates and vapor wall loss effects (Zhang et al., 2014). While it is likely that the SOA yields from the nitrate radical oxidation of various monoterpenes are different (Fry et al., 2014), updating SOA formation from β-pinene+NO_3 with the new yield parameters in future modeling studies would lead to a more accurate prediction of the amount of aerosol formed from this reaction pathway.

Currently, the fate of peroxy radicals (RO_2+HO_2 vs RO_2+NO_3, etc) in the nighttime atmosphere is still highly uncertain (Brown and Stutz, 2012), though recent studies showed that the HO_2 mixing ratio is often on the order of 10 ppt (Mao et al., 2012). Thus, RO_2+HO_2 could be the dominant nighttime fate of peroxy radicals. In this study, we examine the effect of RO_2 fate on aerosol yields for the β-pinene+NO_3 system. Although more ROOH species are produced through the RO_2+HO_2 channel, the SOA yields in the "RO_2+NO_3 dominant" and "RO_2+HO_2 dominant" experiments are comparable. This indicates that for this system, the overall product chemical composition and volatility distribution may not be very different for the different peroxy radical fates. This is in contrast to results from nitrate radical oxidation of smaller biogenic species, such as isoprene, which have large differences in SOA yields depending on the RO_2 fate (Ng et al., 2008). This suggests that the fates of peroxy radicals in nitrate radical experiments for larger BVOCs (such as monoterpenes and sesquiterpenes) may not be as important as it is for small compounds (such as isoprene) and in photooxidation and ozonolysis experiments (e.g., Presto et al., 2005; Kroll et al., 2006; Ng et al., 2007b; Eddingsaas et al., 2012; Xu et al., 2014). This warrants further studies.

The results from this study provide the first insight for the specific organic nitrate branching ratio on the β-pinene+NO_3 system. We determine that about 90 and 10% of the organic nitrates formed from the β-pinene+NO_3 reaction are primary organic nitrates and tertiary organic nitrates, respectively. As primary and tertiary organic nitrates hydrolyze at drastically different rates, the relative contribution of primary vs. tertiary organic nitrates determined in this work would allow for improved constraints regarding the fates of organic nitrates in the atmosphere. Specifically, we find that the primary organic nitrates do not appear to hydrolyze and the tertiary organic nitrates undergo hydrolysis with a lifetime of 3-4.5 hours. Updating the branching ratio (primary vs. tertiary) with organic nitrates formed by the NO_3-initiated oxidation of BVOCs will improve model predictions of hydrolysis of organic nitrates. Hydrolysis of organic nitrates has the potential to create a long term sink for atmospheric nitrogen in the form of nitric acid. Organic nitrates that do not hydrolyze, however, can potentially be photolyzed or oxidized by OH radicals to release NO_x back into the atmosphere (Suarez-Bertoa et al., 2012) or lost by dry or wet deposition.

Results from this chamber study are used to evaluate the contributions from the nitrate radical oxidation of BVOCs to ambient OA in the southeastern United States, where this chemistry is expected to be substantial owing to high natural and anthropogenic emissions in the area. Factor analysis of HR-ToF-AMS data from SOAS and SCAPE field measurements identified an OA subtype (LO-OOA) at these sites which is highly correlated with organic nitrates (Xu et al., 2015a, b). The β-pinene+NO_3 SOA yields obtained under reaction conditions relevant to these field studies are directly utilized to estimate the amount of ambient OA formed from this reaction pathway (Xu et al., 2015b). Specifically, it is estimated that 50% of nighttime OA could be produced by the reaction of β-pinene with nitrate radicals in SOAS (Xu et al., 2015b). Results from this study and Xu et al. (2015b) illustrate the substantial insights one can gain into aerosol formation chemistry and ambient aerosol source apportionment through coordinated fundamental laboratory studies and field measurement studies. Further, multiple gas-phase organic nitrate species are identified in this chamber study, which could be used to help interpret ambient gas-phase composition data obtained from the large suite of gas-phase measurements in SOAS. Owing to difficulties in measuring complex atmospheric processes, laboratory studies are critical in generating fundamental data to understand and predict SOA formation regionally and

globally. In this regard, it is imperative not to view laboratory studies as isolated efforts, but instead to make them essential and integrated parts of research activities in the wider atmospheric chemistry community (e.g., field campaigns).

Acknowledgements

This research was funded by US Environmental Protection Agency STAR grant (Early Career) RD-83540301. L. Xu is in part supported by NSF grant 1242258 and US EPA STAR grant R834799. W. Y. Tuet is in part supported by the Health Effects Institute under Research Agreement #4943-RFA13-2/14-4. This publication's contents are solely the responsibility of the grantee and do not necessarily represent the official views of the US EPA. Further, US EPA does not endorse the purchase of any commercial products or services mentioned in the publication. M. I. Guzman wishes to acknowledge support from NSF CAREER award (CHE-1255290). The authors would like to thank X. X. Liu, D. X. Chen, D. J. Tanner and H. G. Huey for use and aid with their chemical ionization mass spectrometer, and to E. C. Wood for helpful discussions on the N_2O_5 injection flow tube design.

References

Akagi, S. K., Yokelson, R. J., Burling, I. R., Meinardi, S., Simpson, I., Blake, D. R., McMeeking, G. R., Sullivan, A., Lee, T., Kreidenweis, S., Urbanski, S., Reardon, J., Griffith, D. W. T., Johnson, T. J., and Weise, D. R.: Measurements of reactive trace gases and variable O3 formation rates in some South Carolina biomass burning plumes, Atmos. Chem. Phys., 13, 1141-1165, doi:10.5194/acp-13-1141-2013, 2013.

Arey, J., Aschmann, S. M., Kwok, E. S. C., and Atkinson, R.: Alkyl Nitrate, Hydroxyalkyl Nitrate, and Hydroxycarbonyl Formation from the NOx−Air Photooxidations of C5−C8 n-Alkanes, The Journal of Physical Chemistry A, 105, 1020-1027, doi:10.1021/jp003292z, 2001.

Atkinson, R.: KINETICS AND MECHANISMS OF THE GAS-PHASE REACTIONS OF THE NO3 RADICAL WITH ORGANIC-COMPOUNDS, Journal of Physical and Chemical Reference Data, 20, 459-507, 1991.

Atkinson, R.: Atmospheric Reactions of Alkoxy and β-Hydroxyalkoxy Radicals, Int. J. Chem. Kinet., 29, 99-111, doi:10.1002/(SICI)1097-4601(1997)29:2<99::AID-KIN3>3.0.CO;2-F, 1997.

Atkinson, R., and Arey, J.: Gas-phase Tropospheric Chemistry of Biogenic Volatile Organic Compounds: A Review, Atmos. Environ., 37, 197-219, 2003a.

1138 Atkinson, R., and Arey, J.: Atmospheric degradation of volatile organic compounds, Chemical
1139 Reviews, 103, 4605-4638, 2003b.

1140 Bahreini, R., Keywood, M. D., Ng, N. L., Varutbangkul, V., Gao, S., Flagan, R. C., Seinfeld, J.
1141 H., Worsnop, D. R., and Jimenez, J. L.: Measurements of Secondary Organic Aerosol from
1142 Oxidation of Cycloalkenes, Terpenes, and m-Xylene Using an Aerodyne Aerosol Mass
1143 Spectrometer, Environ. Sci. Technol., 39, 5674-5688, doi:10.1021/es048061a, 2005.

1144 Beaver, M. R., St Clair, J. M., Paulot, F., Spencer, K. M., Crounse, J. D., LaFranchi, B. W., Min,
1145 K. E., Pusede, S. E., Wooldridge, P. J., Schade, G. W., Park, C., Cohen, R. C., and Wennberg, P.
1146 O.: Importance of biogenic precursors to the budget of organic nitrates: observations of
1147 multifunctional organic nitrates by CIMS and TD-LIF during BEARPEX 2009, Atmos. Chem.
1148 Phys., 12, 5773-5785, doi:10.5194/acp-12-5773-2012, 2012.

1149 Berndt, T., and Boge, O.: Gas-phase reaction of NO3 radicals with isoprene: A kinetic and
1150 mechanistic study, International Journal of Chemical Kinetics, 29, 755-765,
1151 doi:10.1002/(sici)1097-4601(1997)29:10<755::aid-kin4>3.0.co;2-l, 1997a.

1152 Berndt, T., and Boge, O.: Products and mechanism of the gas-phase reaction of NO3 radicals
1153 with alpha-pinene, Journal of the Chemical Society-Faraday Transactions, 93, 3021-3027,
1154 doi:10.1039/a702364b, 1997b.

1155 Bonn, B., and Moorgat, G. K.: New particle formation during a- and b-pinene oxidation by O3,
1156 OH and NO3, and the influence of water vapour: particle size distribution studies, Atmos. Chem.
1157 Phys., 2, 183-196, doi:10.5194/acp-2-183-2002, 2002.

1158 Bowman, F. M., Odum, J. R., Seinfeld, J. H., and Pandis, S. N.: Mathematical model for gas-
1159 particle partitioning of secondary organic aerosols, Atmospheric Environment, 31, 3921-3931,
1160 doi:10.1016/s1352-2310(97)00245-8, 1997.

1161 Brown, S. S., deGouw, J. A., Warneke, C., Ryerson, T. B., Dube, W. P., Atlas, E., Weber, R. J.,
1162 Peltier, R. E., Neuman, J. A., Roberts, J. M., Swanson, A., Flocke, F., McKeen, S. A., Brioude,
1163 J., Sommariva, R., Trainer, M., Fehsenfeld, F. C., and Ravishankara, A. R.: Nocturnal isoprene
1164 oxidation over the Northeast United States in summer and its impact on reactive nitrogen
1165 partitioning and secondary organic aerosol, Atmos. Chem. Phys., 9, 3027-3042, 2009.

1166 Brown, S. S., and Stutz, J.: Nighttime radical observations and chemistry, Chemical Society
1167 Reviews, 41, 6405-6447, doi:10.1039/c2cs35181a, 2012.

1168 Brown, S. S., Dube, W. P., Bahreini, R., Middlebrook, A. M., Brock, C. A., Warneke, C., de
1169 Gouw, J. A., Washenfelder, R. A., Atlas, E., Peischl, J., Ryerson, T. B., Holloway, J. S.,
1170 Schwarz, J. P., Spackman, R., Trainer, M., Parrish, D. D., Fehshenfeld, F. C., and Ravishankara,
1171 A. R.: Biogenic VOC oxidation and organic aerosol formation in an urban nocturnal boundary
1172 layer: aircraft vertical profiles in Houston, TX, Atmos. Chem. Phys., 13, 11317-11337,
1173 doi:10.5194/acp-13-11317-2013, 2013.

1174 Browne, E. C., and Cohen, R. C.: Effects of biogenic nitrate chemistry on the NOx lifetime in
1175 remote continental regions, Atmos. Chem. Phys., 12, 11917-11932, doi:10.5194/acp-12-11917-
1176 2012, 2012.

1177 Browne, E. C., Min, K. E., Wooldridge, P. J., Apel, E., Blake, D. R., Brune, W. H., Cantrell, C.
1178 A., Cubison, M. J., Diskin, G. S., Jimenez, J. L., Weinheimer, A. J., Wennberg, P. O., Wisthaler,
1179 A., and Cohen, R. C.: Observations of total RONO2 over the boreal forest: NOx sinks and
1180 HNO3 sources, Atmos. Chem. Phys., 13, 4543-4562, doi:10.5194/acp-13-4543-2013, 2013.

1181 Browne, E. C., Wooldridge, P. J., Min, K. E., and Cohen, R. C.: On the role of monoterpene
1182 chemistry in the remote continental boundary layer, Atmos. Chem. Phys., 14, 1225-1238,
1183 doi:10.5194/acp-14-1225-2014, 2014.

1184 Bruns, E. A., Perraud, V., Zelenyuk, A., Ezell, M. J., Johnson, S. N., Yu, Y., Imre, D.,
1185 Finlayson-Pitts, B. J., and Alexander, M. L.: Comparison of FTIR and Particle Mass
1186 Spectrometry for the Measurement of Particulate Organic Nitrates, Environ. Sci. Technol., 44,
1187 1056-1061, doi:10.1021/es9029864, 2010.

1188 Canagaratna, M. R., Jimenez, J. L., Kroll, J. H., Chen, Q., Kessler, S. H., Massoli, P.,
1189 Hildebrandt Ruiz, L., Fortner, E., Williams, L. R., Wilson, K. R., Surratt, J. D., Donahue, N. M.,
1190 Jayne, J. T., and Worsnop, D. R.: Elemental ratio measurements of organic compounds using
1191 aerosol mass spectrometry: characterization, improved calibration, and implications, Atmos.
1192 Chem. Phys., 15, 253-272, doi:10.5194/acp-15-253-2015, 2015.

1193 Carter, W. P. L., Darnall, K. R., Lloyd, A. C., Winer, A. M., and Pitts Jr, J. N.: Evidence for
1194 Alkoxy Radical Isomerization in Photooxidations of C_4-C_6 Alkanes under Simulated
1195 Atmospheric Conditions, Chem. Phys. Lett., 42, 22-27, doi:http://dx.doi.org/10.1016/0009-
1196 2614(76)80543-X, 1976.

1197 Cerully, K. M., Bougiatioti, A., Hite, J. R., Guo, H., Xu, L., Ng, N. L., Weber, R. J., and Nenes,
1198 A.: On the Link Between Hygroscopicity, Volatility, and Oxidation State of Ambient and Water-
1199 Soluble Aerosol in the Southeastern United Sates., Atmos. Chem. Phys. Discuss., 14, 30835-
1200 30877, doi:doi:10.5194/acpd-14-30835-2014, 2014.

1201 Chen, Q., Farmer, D. K., Rizzo, L. V., Pauliquevis, T., Kuwata, M., Karl, T. G., Guenther, A.,
1202 Allan, J. D., Coe, H., Andreae, M. O., Pöschl, U., Jimenez, J. L., Artaxo, P., and Martin, S. T.:
1203 Submicron particle mass concentrations and sources in the Amazonian wet season (AMAZE-08),
1204 Atmos. Chem. Phys., 15, 3687-3701, doi:10.5194/acp-15-3687-2015, 2015.

1205 Chen, X., Hulbert, D., and Shepson, P. B.: Measurement of the organic nitrate yield from OH
1206 reaction with isoprene, Journal of Geophysical Research: Atmospheres, 103, 25563-25568,
1207 doi:10.1029/98JD01483, 1998.

1208 Chhabra, P. S., Flagan, R. C., and Seinfeld, J. H.: Elemental analysis of chamber organic aerosol
1209 using an aerodyne high-resolution aerosol mass spectrometer, Atmos. Chem. Phys., 10, 4111-
1210 4131, doi:10.5194/acp-10-4111-2010, 2010.

1211 Chung, S. H., and Seinfeld, J. H.: Global distribution and climate forcing of carbonaceous
1212 aerosols, Journal of Geophysical Research: Atmospheres, 107, 4407,
1213 doi:10.1029/2001JD001397, 2002.

1214 Darer, A. I., Cole-Filipiak, N. C., O'Connor, A. E., and Elrod, M. J.: Formation and Stability of
1215 Atmospherically Relevant Isoprene-Derived Organosulfates and Organonitrates, Environ. Sci.
1216 Technol., 45, 1895-1902, doi:10.1021/es103797z, 2011.

1217 Day, D. A., Liu, S., Russell, L. M., and Ziemann, P. J.: Organonitrate group concentrations in
1218 submicron particles with high nitrate and organic fractions in coastal southern California,
1219 Atmospheric Environment, 44, 1970-1979, doi:10.1016/j.atmosenv.2010.02.045, 2010.

1220 de Gouw, J. A., Middlebrook, A. M., Warneke, C., Goldan, P. D., Kuster, W. C., Roberts, J. M.,
1221 Fehsenfeld, F. C., Worsnop, D. R., Canagaratna, M. R., Pszenny, A. A. P., Keene, W. C.,
1222 Marchewka, M., Bertman, S. B., and Bates, T. S.: Budget of organic carbon in a polluted
1223 atmosphere: Results from the New England Air Quality Study in 2002, Journal of Geophysical
1224 Research-Atmospheres, 110, D16305, doi:16310.11029/12004JD005623, 2005.

1225 DeCarlo, P. F., Kimmel, J. R., Trimborn, A., Northway, M. J., Jayne, J. T., Aiken, A. C., Gonin,
1226 M., Fuhrer, K., Horvath, T., Docherty, K. S., Worsnop, D. R., and Jimenez, J. L.: Field-
1227 deployable, high-resolution, time-of-flight aerosol mass spectrometer, Analytical Chemistry, 78,
1228 8281-8289, doi:10.1021/ac061249n, 2006.

1229 Dibble, T. S.: Reactions of the alkoxy radicals formed following OH-addition to alpha-pinene
1230 and beta-pinene. C-C bond scission reactions, Journal of the American Chemical Society, 123,
1231 4228-4234, doi:10.1021/ja003553i, 2001.

1232 Dillon, T. J., and Crowley, J. N.: Direct detection of OH formation in the reactions of HO(2)
1233 with CH(3)C(O)O(2) and other substituted peroxy radicals, Atmos. Chem. Phys., 8, 4877-4889,
1234 2008.

1235 Donahue, N. M., Robinson, A. L., Stanier, C. O., and Pandis, S. N.: Coupled partitioning,
1236 dilution, and chemical aging of semivolatile organics, Environ. Sci. Technol., 40, 2635-2643,
1237 doi:10.1021/es052297c, 2006.

1238 Donahue, N. M., Henry, K. M., Mentel, T. F., Kiendler-Scharr, A., Spindler, C., Bohn, B.,
1239 Brauers, T., Dorn, H. P., Fuchs, H., Tillmann, R., Wahner, A., Saathoff, H., Naumann, K.-H.,
1240 Moehler, O., Leisner, T., Mueller, L., Reinnig, M.-C., Hoffmann, T., Salo, K., Hallquist, M.,
1241 Frosch, M., Bilde, M., Tritscher, T., Barmet, P., Praplan, A. P., DeCarlo, P. F., Dommen, J.,
1242 Prevot, A. S. H., and Baltensperger, U.: Aging of biogenic secondary organic aerosol via gas-
1243 phase OH radical reactions, Proceedings of the National Academy of Sciences of the United
1244 States of America, 109, 13503-13508, doi:10.1073/pnas.1115186109, 2012.

1245 Duplissy, J., DeCarlo, P. F., Dommen, J., Alfarra, M. R., Metzger, A., Barmpadimos, I., Prevot,
1246 A. S. H., Weingartner, E., Tritscher, T., Gysel, M., Aiken, A. C., Jimenez, J. L., Canagaratna, M.
1247 R., Worsnop, D. R., Collins, D. R., Tomlinson, J., and Baltensperger, U.: Relating
1248 hygroscopicity and composition of organic aerosol particulate matter, Atmos. Chem. Phys., 11,
1249 1155-1165, doi:10.5194/acp-11-1155-2011, 2011.

1250 Eberhard, J., Muller, C., Stocker, D. W., and Kerr, J. A.: Isomerization of Alkoxy Radicals under
1251 Atmospheric Conditions, Environ. Sci. Technol., 29, 232-241, doi:10.1021/es00001a600, 1995.

1252 Eddingsaas, N. C., Loza, C. L., Yee, L. D., Seinfeld, J. H., and Wennberg, P. O.: alpha-pinene
1253 photooxidation under controlled chemical conditions - Part 1: Gas-phase composition in low-
1254 and high-NOx environments, Atmos. Chem. Phys., 12, 6489-6504, doi:10.5194/acp-12-6489-
1255 2012, 2012.

1256 Ervens, B., Turpin, B. J., and Weber, R. J.: Secondary organic aerosol formation in cloud
1257 droplets and aqueous particles (aqSOA): a review of laboratory, field and model studies, Atmos.
1258 Chem. Phys., 11, 11069-11102, doi:10.5194/acp-11-11069-2011, 2011.

1259 Farmer, D. K., Matsunaga, A., Docherty, K. S., Surratt, J. D., Seinfeld, J. H., Ziemann, P. J., and
1260 Jimenez, J. L.: Response of an aerosol mass spectrometer to organonitrates and organosulfates
1261 and implications for atmospheric chemistry, Proceedings of the National Academy of Sciences
1262 of the United States of America, 107, 6670-6675, doi:10.1073/pnas.0912340107, 2010.

1263 Farmer, E. H., Koch, H. P., and Sutton, D. A.: The Course of Autoxidation Reactions in
1264 Polyisoprenes and Allied Compounds. Part VII. Rearrangement of Double Bonds During
1265 Autoxidation, J. Chem. Soc., 541-547, doi:10.1039/JR9430000541, 1943.

1266 Fry, J. L., Kiendler-Scharr, A., Rollins, A. W., Wooldridge, P. J., Brown, S. S., Fuchs, H., Dubé,
1267 W., Mensah, A., dal Maso, M., Tillmann, R., Dorn, H. P., Brauers, T., and Cohen, R. C.: Organic
1268 nitrate and secondary organic aerosol yield from NO3 oxidation of β-pinene evaluated using a
1269 gas-phase kinetics/aerosol partitioning model, Atmos. Chem. Phys., 9, 1431-1449,
1270 doi:10.5194/acp-9-1431-2009, 2009.

1271 Fry, J. L., Kiendler-Scharr, A., Rollins, A. W., Brauers, T., Brown, S. S., Dorn, H. P., Dubé, W.
1272 P., Fuchs, H., Mensah, A., Rohrer, F., Tillmann, R., Wahner, A., Wooldridge, P. J., and Cohen,
1273 R. C.: SOA from limonene: role of NO3 in its generation and degradation, Atmos. Chem. Phys.,
1274 11, 3879-3894, doi:10.5194/acp-11-3879-2011, 2011.

1275 Fry, J. L., Draper, D. C., Zarzana, K. J., Campuzano-Jost, P., Day, D. A., Jimenez, J. L., Brown,
1276 S. S., Cohen, R. C., Kaser, L., Hansel, A., Cappellin, L., Karl, T., Roux, A. H., Turnipseed, A.,
1277 Cantrell, C., Lefer, B. L., and Grossberg, N.: Observations of gas- and aerosol-phase organic
1278 nitrates at BEACHON-RoMBAS 2011, Atmos. Chem. Phys., 13, 8585-8605, doi:10.5194/acp-
1279 13-8585-2013, 2013.

1280 Fry, J. L., Draper, D. C., Barsanti, K. C., Smith, J. N., Ortega, J., Winkler, P. M., Lawler, M. J.,
1281 Brown, S. S., Edwards, P. M., Cohen, R. C., and Lee, L.: Secondary Organic Aerosol Formation
1282 and Organic Nitrate Yield from NO3 Oxidation of Biogenic Hydrocarbons, Environ. Sci.
1283 Technol., 48, 11944-11953, doi:10.1021/es502204x, 2014.

1284 Fuentes, J., Wang, D., Bowling, D., Potosnak, M., Monson, R., Goliff, W., and Stockwell, W.:
1285 Biogenic Hydrocarbon Chemistry within and Above a Mixed Deciduous Forest, Journal of
1286 Atmospheric Chemistry, 56, 165-185, doi:10.1007/s10874-006-9048-4, 2007.

Fuentes, J. D., Lerdau, M., Atkinson, R., Baldocchi, D., Bottenheim, J. W., Ciccioli, P., Lamb, B., Geron, C., Gu, L., Guenther, A., Sharkey, T. D., and Stockwell, W.: Biogenic hydrocarbons in the atmospheric boundary layer: A review, Bull. Amer. Meteorol. Soc., 81, 1537-1575, doi:10.1175/1520-0477(2000)081<1537:bhitab>2.3.co;2, 2000.

Gao, S., Ng, N. L., Keywood, M., Varutbangkul, V., Bahreini, R., Nenes, A., He, J., Yoo, K. Y., Beauchamp, J. L., Hodyss, R. P., Flagan, R. C., and Seinfeld, J. H.: Particle Phase Acidity and Oligomer Formation in Secondary Organic Aerosol, Environ. Sci. Technol., 38, 6582-6589, doi:10.1021/es049125k, 2004.

Gaston, C. J., Thornton, J. A., and Ng, N. L.: Reactive uptake of N2O5 to internally mixed inorganic and organic particles: the role of organic carbon oxidation state and inferred organic phase separations, Atmos. Chem. Phys., 14, 5693-5707, doi:10.5194/acp-14-5693-2014, 2014.

Griffin, R. J., Cocker, D. R., Flagan, R. C., and Seinfeld, J. H.: Organic aerosol formation from the oxidation of biogenic hydrocarbons, Journal of Geophysical Research-Atmospheres, 104, 3555-3567, doi:10.1029/1998jd100049, 1999.

Guenther, A. B., Jiang, X., Heald, C. L., Sakulyanontvittaya, T., Duhl, T., Emmons, L. K., and Wang, X.: The Model of Emissions of Gases and Aerosols from Nature version 2.1 (MEGAN2.1): an extended and updated framework for modeling biogenic emissions, Geoscientific Model Development, 5, 1471-1492, doi:10.5194/gmd-5-1471-2012, 2012.

Guo, H., Xu, L., Bougiatioti, A., Cerully, K. M., Capps, S. L., Hite Jr, J. R., Carlton, A. G., Lee, S. H., Bergin, M. H., Ng, N. L., Nenes, A., and Weber, R. J.: Fine-particle water and pH in the southeastern United States, Atmos. Chem. Phys., 15, 5211-5228, doi:10.5194/acp-15-5211-2015, 2015.

Hallquist, M., Wangberg, I., Ljungstrom, E., Barnes, I., and Becker, K. H.: Aerosol and product yields from NO3 radical-initiated oxidation of selected monoterpenes, Environ. Sci. Technol., 33, 553-559, doi:10.1021/es980292s, 1999.

Hasson, A. S., Tyndall, G. S., Orlando, J. J., Singh, S., Hernandez, S. Q., Campbell, S., and Ibarra, Y.: Branching Ratios for the Reaction of Selected Carbonyl-Containing Peroxy Radicals with Hydroperoxy Radicals, The Journal of Physical Chemistry A, 116, 6264-6281, doi:10.1021/jp211799c, 2012.

Hatch, L. E., Luo, W., Pankow, J. F., Yokelson, R. J., Stockwell, C. E., and Barsanti, K. C.: Identification and quantification of gaseous organic compounds emitted from biomass burning using two-dimensional gas chromatography-time-of-flight mass spectrometry, Atmos. Chem. Phys., 15, 1865-1899, doi:10.5194/acp-15-1865-2015, 2015.

Henry, K. M., and Donahue, N. M.: Photochemical Aging of α-Pinene Secondary Organic Aerosol: Effects of OH Radical Sources and Photolysis, The Journal of Physical Chemistry A, 116, 5932-5940, doi:10.1021/jp210288s, 2012.

1323 Hoyle, C. R., Berntsen, T., Myhre, G., and Isaksen, I. S. A.: Secondary organic aerosol in the
1324 global aerosol – chemical transport model Oslo CTM2, Atmos. Chem. Phys., 7, 5675-
1325 5694, doi:10.5194/acp-7-5675-2007, 2007.

1326 Hu, K. S., Darer, A. I., and Elrod, M. J.: Thermodynamics and kinetics of the hydrolysis of
1327 atmospherically relevant organonitrates and organosulfates, Atmos. Chem. Phys., 11, 8307-8320,
1328 doi:10.5194/acp-11-8307-2011, 2011.

1329 Huey, L. G.: Measurement of trace atmospheric species by chemical ionization mass
1330 spectrometry: Speciation of reactive nitrogen and future directions, Mass Spectrom. Rev., 26,
1331 166-184, doi:10.1002/mas.20118, 2007.

1332 Iinuma, Y., Muller, C., Berndt, T., Boge, O., Claeys, M., and Herrmann, H.: Evidence for the
1333 existence of organosulfates from beta-pinene ozonolysis in ambient secondary organic aerosol,
1334 Environ. Sci. Technol., 41, 6678-6683, doi:10.1021/es070938t, 2007.

1335 Jacobs, M. I., Burke, W. J., and Elrod, M. J.: Kinetics of the reactions of isoprene-derived
1336 hydroxynitrates: gas phase epoxide formation and solution phase hydrolysis, Atmos. Chem.
1337 Phys., 14, 8933-8946, doi:10.5194/acp-14-8933-2014, 2014.

1338 Jaoui, M., Kleindienst, T. E., Docherty, K. S., Lewandowski, M., and Offenberg, J. H.:
1339 Secondary organic aerosol formation from the oxidation of a series of sesquiterpenes: alpha-
1340 cedrene, beta-caryophyllene, alpha-humulene and alpha-farnesene with O-3, OH and NO3
1341 radicals, Environmental Chemistry, 10, 178-193, doi:10.1071/en13025, 2013.

1342 Jenkin, M. E., Hurley, M. D., and Wallington, T. J.: Investigation of the radical product channel
1343 of the CH3C(O)O2 + HO2 reaction in the gas phase, Physical Chemistry Chemical Physics, 9,
1344 3149-3162, doi:10.1039/B702757E, 2007.

1345 Kanakidou, M., Seinfeld, J. H., Pandis, S. N., Barnes, I., Dentener, F. J., Facchini, M. C., Van
1346 Dingenen, R., Ervens, B., Nenes, A., Nielsen, C. J., Swietlicki, E., Putaud, J. P., Balkanski, Y.,
1347 Fuzzi, S., Horth, J., Moortgat, G. K., Winterhalter, R., Myhre, C. E. L., Tsigaridis, K., Vignati,
1348 E., Stephanou, E. G., and Wilson, J.: Organic aerosol and global climate modelling: a review,
1349 Atmos. Chem. Phys., 5, 1053-1123, 2005.

1350 Kerdouci, J., Picquet-Varrault, B., and Doussin, J. F.: Prediction of Rate Constants for Gas-Phase
1351 Reactions of Nitrate Radical with Organic Compounds: A New Structure-Activity Relationship,
1352 ChemPhysChem, 11, 3909-3920, doi:10.1002/cphc.201000673, 2010.

1353 Kerdouci, J., Picquet-Varrault, B., and Doussin, J. F.: Structure-activity relationship for the gas-
1354 phase reactions of NO3 radical with organic compounds: Update and extension to aldehydes,
1355 Atmospheric Environment, 84, 363-372, doi:10.1016/j.atmosenv.2013.11.024, 2014.

1356 Keywood, M. D., Varutbangkul, V., Bahreini, R., Flagan, R. C., and Seinfeld, J. H.: Secondary
1357 organic aerosol formation from the ozonolysis of cycloalkenes and related compounds, Environ.
1358 Sci. Technol., 38, 4157-4164, doi:10.1021/es035363o, 2004.

1359 Kirchner, F., and Stockwell, W. R.: Effect of peroxy radical reactions on the predicted
1360 concentrations of ozone, nitrogenous compounds, and radicals, Journal of Geophysical Research:
1361 Atmospheres, 101, 21007-21022, doi:10.1029/96JD01519, 1996.

1362 Kroll, J. H., Ng, N. L., Murphy, S. M., Flagan, R. C., and Seinfeld, J. H.: Secondary Organic
1363 Aerosol Formation from Isoprene Photooxidation, Environ. Sci. Technol., 40, 1869-1877,
1364 doi:10.1021/es0524301, 2006.

1365 Kroll, J. H., and Seinfeld, J. H.: Chemistry of secondary organic aerosol: Formation and
1366 evolution of low-volatility organics in the atmosphere, Atmospheric Environment, 42, 3593-
1367 3624, doi:10.1016/j.atmosenv.2008.01.003, 2008.

1368 Kroll, J. H., Smith, J. D., Che, D. L., Kessler, S. H., Worsnop, D. R., and Wilson, K. R.:
1369 Measurement of fragmentation and functionalization pathways in the heterogeneous oxidation of
1370 oxidized organic aerosol, Physical Chemistry Chemical Physics, 11, 8005-8014,
1371 doi:10.1039/b905289e, 2009.

1372 Kwan, A. J., Chan, A. W. H., Ng, N. L., Kjaergaard, H. G., Seinfeld, J. H., and Wennberg, P. O.:
1373 Peroxy radical chemistry and OH radical production during the NO3-initiated oxidation of
1374 isoprene, Atmos. Chem. Phys., 12, 7499-7515, doi:10.5194/acp-12-7499-2012, 2012.

1375 Lewis, C. W., Klouda, G. A., and Ellenson, W. D.: Radiocarbon measurement of the biogenic
1376 contribution to summertime PM-2.5 ambient aerosol in Nashville, TN, Atmospheric
1377 Environment, 38, 6053-6061, doi:http://dx.doi.org/10.1016/j.atmosenv.2004.06.011, 2004.

1378 Li, Y., Chen, Q., Guzman, M., Chan, C., and Martin, S.: Second-generation products contribute
1379 substantially to the particle-phase organic material produced by β-caryophyllene ozonolysis,
1380 Atmos. Chem. Phys., 11, 121-132, 2011.

1381 Liu, S., Shilling, J. E., Song, C., Hiranuma, N., Zaveri, R. A., and Russell, L. M.: Hydrolysis of
1382 Organonitrate Functional Groups in Aerosol Particles, Aerosol Sci. Technol., 46, 1359-1369,
1383 doi:10.1080/02786826.2012.716175, 2012.

1384 Loza, C. L., Chan, A. W. H., Galloway, M. M., Keutsch, F. N., Flagan, R. C., and Seinfeld, J. H.:
1385 Characterization of Vapor Wall Loss in Laboratory Chambers, Environ. Sci. Technol., 44, 5074-
1386 5078, doi:10.1021/es100727v, 2010.

1387 Loza, C. L., Chhabra, P. S., Yee, L. D., Craven, J. S., Flagan, R. C., and Seinfeld, J. H.:
1388 Chemical aging of m-xylene secondary organic aerosol: laboratory chamber study, Atmos.
1389 Chem. Phys., 12, 151-167, doi:10.5194/acp-12-151-2012, 2012.

1390 Mao, J., Ren, X., Zhang, L., Van Duin, D. M., Cohen, R. C., Park, J. H., Goldstein, A. H.,
1391 Paulot, F., Beaver, M. R., Crounse, J. D., Wennberg, P. O., DiGangi, J. P., Henry, S. B.,
1392 Keutsch, F. N., Park, C., Schade, G. W., Wolfe, G. M., Thornton, J. A., and Brune, W. H.:
1393 Insights into hydroxyl measurements and atmospheric oxidation in a California forest, Atmos.
1394 Chem. Phys., 12, 8009-8020, doi:10.5194/acp-12-8009-2012, 2012.

Marley, N. A., Gaffney, J. S., Tackett, M., Sturchio, N. C., Heraty, L., Martinez, N., Hardy, K. D., Marchany-Rivera, A., Guilderson, T., MacMillan, A., and Steelman, K.: The impact of biogenic carbon sources on aerosol absorption in Mexico City, Atmospheric Chemistry and Physics, 9, 1537-1549, 2009.

Matsunaga, A., and Ziemann, P. J.: Yields of beta-hydroxynitrates, dihydroxynitrates, and trihydroxynitrates formed from OH radical-initiated reactions of 2-methyl-1-alkenes, Proceedings of the National Academy of Sciences of the United States of America, 107, 6664-6669, doi:10.1073/pnas.0910585107, 2010.

McLaren, R., Salmon, R. A., Liggio, J., Hayden, K. L., Anlauf, K. G., and Leaitch, W. R.: Nighttime chemistry at a rural site in the Lower Fraser Valley, Atmospheric Environment, 38, 5837-5848, doi:10.1016/j.atmosenv.2004.03.074, 2004.

McNeill, V. F., Wolfe, G. M., and Thornton, J. A.: The Oxidation of Oleate in Submicron Aqueous Salt Aerosols: Evidence of a Surface Process, The Journal of Physical Chemistry A, 111, 1073-1083, doi:10.1021/jp066233f, 2007.

Miller, B.: Advanced Organic Chemistry: Reactions and Mechanisms, Journal of Chemical Education, 76, p. 320, doi:10.1021/ed076p320.2, 1999.

Miller, B.: Advanced Organic Chemistry: Reactions and Mechanisms, 2nd ed., Pearson/Prentice Hall, Lebanon, IN, 2003.

Ng, N. L., Kroll, J. H., Chan, A. W. H., Chhabra, P. S., Flagan, R. C., and Seinfeld, J. H.: Secondary organic aerosol formation from m-xylene, toluene, and benzene, Atmos. Chem. Phys., 7, 3909-3922, doi:10.5194/acp-7-3909-2007, 2007a.

Ng, N. L., Chhabra, P. S., Chan, A. W. H., Surratt, J. D., Kroll, J. H., Kwan, A. J., McCabe, D. C., Wennberg, P. O., Sorooshian, A., Murphy, S. M., Dalleska, N. F., Flagan, R. C., and Seinfeld, J. H.: Effect of NOx level on secondary organic aerosol (SOA) formation from the photooxidation of terpenes, Atmos. Chem. Phys., 7, 5159-5174, 2007b.

Ng, N. L., Kwan, A. J., Surratt, J. D., Chan, A. W. H., Chhabra, P. S., Sorooshian, A., Pye, H. O. T., Crounse, J. D., Wennberg, P. O., Flagan, R. C., and Seinfeld, J. H.: Secondary organic aerosol (SOA) formation from reaction of isoprene with nitrate radicals (NO3), Atmos. Chem. Phys., 8, 4117-4140, 2008.

Ng, N. L., Canagaratna, M. R., Jimenez, J. L., Chhabra, P. S., Seinfeld, J. H., and Worsnop, D. R.: Changes in organic aerosol composition with aging inferred from aerosol mass spectra, Atmos. Chem. Phys., 11, 6465-6474, doi:10.5194/acp-11-6465-2011, 2011.

Nguyen, T. B., Roach, P. J., Laskin, J., Laskin, A., and Nizkorodov, S. A.: Effect of humidity on the composition of isoprene photooxidation secondary organic aerosol, Atmos. Chem. Phys., 11, 6931-6944, doi:DOI 10.5194/acp-11-6931-2011, 2011.

Nguyen, T. B., Crounse, J. D., Schwantes, R. H., Teng, A. P., Bates, K. H., Zhang, X., St. Clair, J. M., Brune, W. H., Tyndall, G. S., Keutsch, F. N., Seinfeld, J. H., and Wennberg, P. O.:

1433 Overview of the Focused Isoprene eXperiment at the California Institute of Technology
1434 (FIXCIT): mechanistic chamber studies on the oxidation of biogenic compounds, Atmos. Chem.
1435 Phys., 14, 13531-13549, doi:10.5194/acp-14-13531-2014, 2014.

1436 Odum, J. R., Hoffmann, T., Bowman, F., Collins, D., Flagan, R. C., and Seinfeld, J. H.:
1437 Gas/Particle Partitioning and Secondary Organic Aerosol Yields, Environ. Sci. Technol., 30,
1438 2580-2585, doi:10.1021/es950943+, 1996.

1439 Odum, J. R., Jungkamp, T. P. W., Griffin, R. J., Flagan, R. C., and Seinfeld, J. H.: The
1440 atmospheric aerosol-forming potential of whole gasoline vapor, Science, 276, 96-99,
1441 doi:10.1126/science.276.5309.96, 1997a.

1442 Odum, J. R., Jungkamp, T. P. W., Griffin, R. J., Forstner, H. J. L., Flagan, R. C., and Seinfeld, J.
1443 H.: Aromatics, reformulated gasoline, and atmospheric organic aerosol formation, Environ. Sci.
1444 Technol., 31, 1890-1897, doi:10.1021/es960535l, 1997b.

1445 Orlando, J. J., and Tyndall, G. S.: Laboratory studies of organic peroxy radical chemistry: an
1446 overview with emphasis on recent issues of atmospheric significance, Chemical Society
1447 Reviews, 41, 6294-6317, doi:10.1039/C2CS35166H, 2012.

1448 Ouchi, A., Liu, C., Kaneda, M., and Hyugano, T.: Photochemical C–C Bond Formation between
1449 Alcohols and Olefins by an Environmentally Benign Radical Reaction, Eur. J. Org. Chem., 2013,
1450 3807-3816, doi:10.1002/ejoc.201300115, 2013.

1451 Pankow, J. F., and Asher, W. E.: SIMPOL.1: a simple group contribution method for predicting
1452 vapor pressures and enthalpies of vaporization of multifunctional organic compounds, Atmos.
1453 Chem. Phys., 8, 2773-2796, 2008.

1454 Pavia, D., Lampman, G., Kriz, G., and Vyvyan, J.: Introduction to spectroscopy, Cengage
1455 Learning, 2008.

1456 Perraud, V., Bruns, E. A., Ezell, M. J., Johnson, S. N., Greaves, J., and Finlayson-Pitts, B. J.:
1457 Identification of Organic Nitrates in the NO3 Radical Initiated Oxidation of α-Pinene by
1458 Atmospheric Pressure Chemical Ionization Mass Spectrometry, Environ. Sci. Technol., 44,
1459 5887-5893, doi:10.1021/es1005658, 2010.

1460 Perring, A. E., Wisthaler, A., Graus, M., Wooldridge, P. J., Lockwood, A. L., Mielke, L. H.,
1461 Shepson, P. B., Hansel, A., and Cohen, R. C.: A product study of the isoprene+NO3 reaction,
1462 Atmos. Chem. Phys., 9, 4945-4956, doi:10.5194/acp-9-4945-2009, 2009.

1463 Presto, A. A., Huff Hartz, K. E., and Donahue, N. M.: Secondary Organic Aerosol Production
1464 from Terpene Ozonolysis. 2. Effect of NOx Concentration, Environ. Sci. Technol., 39, 7046-
1465 7054, doi:10.1021/es050400s, 2005.

1466 Presto, A. A., and Donahue, N. M.: Investigation of alpha-pinene plus ozone secondary organic
1467 aerosol formation at low total aerosol mass, Environ. Sci. Technol., 40, 3536-3543,
1468 doi:10.1021/es052203z, 2006.

1469 Pye, H. O. T., Chan, A. W. H., Barkley, M. P., and Seinfeld, J. H.: Global modeling of organic
1470 aerosol: the importance of reactive nitrogen (NOx and NO3), Atmos. Chem. Phys., 10, 11261-
1471 11276, doi:10.5194/acp-10-11261-2010, 2010.

1472 Qi, L., Nakao, S., and Cocker, D. R., III: Aging of secondary organic aerosol from alpha-pinene
1473 ozonolysis: Roles of hydroxyl and nitrate radicals, Journal of the Air & Waste Management
1474 Association, 62, 1359-1369, doi:10.1080/10962247.2012.712082, 2012.

1475 Rastogi, N., Zhang, X. L., Edgerton, E. S., Ingall, E., and Weber, R. J.: Filterable water-soluble
1476 organic nitrogen in fine particles over the southeastern USA during summer, Atmospheric
1477 Environment, 45, 6040-6047, doi:10.1016/j.atmosenv.2011.07.045, 2011.

1478 Rayez, M.-T., Rayez, J.-C., Kerdouci, J., and Picquet-Varrault, B.: Theoretical Study of the Gas-
1479 Phase Reactions of NO3 Radical with a Series of trans-2-Unsaturated Aldehydes: From Acrolein
1480 to trans-2-Octenal, The Journal of Physical Chemistry A, 118, 5149-5155,
1481 doi:10.1021/jp503619d, 2014.

1482 Rindelaub, J. D., McAvey, K. M., and Shepson, P. B.: The photochemical production of organic
1483 nitrates from α-pinene and loss via acid-dependent particle phase hydrolysis, Atmospheric
1484 Environment, 100, 193-201, doi:http://dx.doi.org/10.1016/j.atmosenv.2014.11.010, 2015.

1485 Rollins, A. W., Kiendler-Scharr, A., Fry, J. L., Brauers, T., Brown, S. S., Dorn, H. P., Dube, W.
1486 P., Fuchs, H., Mensah, A., Mentel, T. F., Rohrer, F., Tillmann, R., Wegener, R., Wooldridge, P.
1487 J., and Cohen, R. C.: Isoprene oxidation by nitrate radical: alkyl nitrate and secondary organic
1488 aerosol yields, Atmos. Chem. Phys., 9, 6685-6703, 2009.

1489 Rollins, A. W., Browne, E. C., Min, K. E., Pusede, S. E., Wooldridge, P. J., Gentner, D. R.,
1490 Goldstein, A. H., Liu, S., Day, D. A., Russell, L. M., and Cohen, R. C.: Evidence for NOx
1491 Control over Nighttime SOA Formation, Science, 337, 1210-1212,
1492 doi:10.1126/science.1221520, 2012.

1493 Rollins, A. W., Pusede, S., Wooldridge, P., Min, K. E., Gentner, D. R., Goldstein, A. H., Liu, S.,
1494 Day, D. A., Russell, L. M., Rubitschun, C. L., Surratt, J. D., and Cohen, R. C.: Gas/particle
1495 partitioning of total alkyl nitrates observed with TD-LIF in Bakersfield, Journal of Geophysical
1496 Research-Atmospheres, 118, 6651-6662, doi:10.1002/jgrd.50522, 2013.

1497 Russell, G. A.: Deuterium-isotope Effects in the Autoxidation of Aralkyl Hydrocarbons.
1498 Mechanism of the Interaction of Peroxy Radicals, J. Am. Cgem. Soc., 79, 3871-3877,
1499 doi:10.1021/ja01571a068, 1957.

1500 Russell, M., and Allen, D. T.: Predicting secondary organic aerosol formation rates in southeast
1501 Texas, Journal of Geophysical Research: Atmospheres, 110, D07S17,
1502 doi:10.1029/2004JD004722, 2005.

1503 Sato, K.: Detection of nitrooxypolyols in secondary organic aerosol formed from the
1504 photooxidation of conjugated dienes under high-NOx conditions, Atmospheric Environment, 42,
1505 6851-6861, doi:10.1016/j.atmosenv.2008.05.010, 2008.

Saunders, S. M., Jenkin, M. E., Derwent, R. G., and Pilling, M. J.: Protocol for the development of the Master Chemical Mechanism, MCM v3 (Part A): tropospheric degradation of non-aromatic volatile organic compounds, Atmos. Chem. Phys., 3, 161-180, 2003.

Schichtel, B. A., Malm, W. C., Bench, G., Fallon, S., McDade, C. E., Chow, J. C., and Watson, J. G.: Fossil and contemporary fine particulate carbon fractions at 12 rural and urban sites in the United States, Journal of Geophysical Research: Atmospheres, 113, D02311, doi:10.1029/2007JD008605, 2008.

Schröder, K., Junge, K., Spannenberg, A., and Beller, M.: Design of a bio-inspired imidazole-based iron catalyst for epoxidation of olefins: Mechanistic insights, Catalysis Today, 157, 364-370, doi:10.1016/j.cattod.2010.04.034, 2010.

Slusher, D. L., Huey, L. G., Tanner, D. J., Flocke, F. M., and Roberts, J. M.: A thermal dissociation–chemical ionization mass spectrometry (TD-CIMS) technique for the simultaneous measurement of peroxyacyl nitrates and dinitrogen pentoxide, Journal of Geophysical Research: Atmospheres, 109, D19315, doi:10.1029/2004JD004670, 2004.

Spittler, M., Barnes, I., Bejan, I., Brockmann, K. J., Benter, T., and Wirtz, K.: Reactions of NO3 radicals with limonene and alpha-pinene: Product and SOA formation, Atmospheric Environment, 40, S116-S127, doi:10.1016/j.atmosenv.2005.09.093, 2006.

Stockwell, C. E., Veres, P. R., Williams, J., and Yokelson, R. J.: Characterization of biomass burning emissions from cooking fires, peat, crop residue, and other fuels with high-resolution proton-transfer-reaction time-of-flight mass spectrometry, Atmos. Chem. Phys., 15, 845-865, doi:10.5194/acp-15-845-2015, 2015.

Stolle, A., Ondruschka, B., and Hopf, H.: Thermal Rearrangements of Monoterpenes and Monoterpenoids, Helvetica Chimica Acta, 92, 1673-1719, doi:10.1002/hlca.200900041, 2009.

Suarez-Bertoa, R., Picquet-Varrault, B., Tamas, W., Pangui, E., and Doussin, J. F.: Atmospheric Fate of a Series of Carbonyl Nitrates: Photolysis Frequencies and OH-Oxidation Rate Constants, Environ. Sci. Technol., 46, 12502-12509, doi:10.1021/es302613x, 2012.

Surratt, J. D., Lewandowski, M., Offenberg, J. H., Jaoui, M., Kleindienst, T. E., Edney, E. O., and Seinfeld, J. H.: Effect of Acidity on Secondary Organic Aerosol Formation from Isoprene, Environ. Sci. Technol., 41, 5363-5369, doi:10.1021/es0704176, 2007.

Szmigielski, R., Vermeylen, R., Dommen, J., Metzger, A., Maenhaut, W., Baltensperger, U., and Claeys, M.: The acid effect in the formation of 2-methyltetrols from the photooxidation of isoprene in the presence of NOx, Atmospheric Research, 98, 183-189, doi:http://dx.doi.org/10.1016/j.atmosres.2010.02.012, 2010.

Thornton, J. A., Braban, C. F., and Abbatt, J. P. D.: N2O5 hydrolysis on sub-micron organic aerosols: the effect of relative humidity, particle phase, and particle size, Physical Chemistry Chemical Physics, 5, 4593-4603, doi:10.1039/B307498F, 2003.

Turrà, N., Neuenschwander, U., Baiker, A., Peeters, J., and Hermans, I.: Mechanism of the Catalytic Deperoxidation of tert-Butylhydroperoxide with Cobalt(II) Acetylacetonate, Chem.-Eur. J., 16, 13226-13235, doi:10.1002/chem.201000489, 2010.

Vereecken, L., and Peeters, J.: Nontraditional (Per)oxy Ring-Closure Paths in the Atmospheric Oxidation of Isoprene and Monoterpenes, J. Phys. Chem. A, 108, 5197-5204, doi:10.1021/jp049219g, 2004.

Vereecken, L., and Peeters, J.: A Theoretical Study of the OH-initiated Gas-phase Oxidation Mechanism of β-pinene ($C_{10}H_{16}$): First Generation Products, Phys. Chem. Chem. Phys., 14, 3802-3815, doi:10.1039/C2CP23711C, 2012.

Verma, V., Fang, T., Guo, H., King, L., Bates, J. T., Peltier, R. E., Edgerton, E., Russell, A. G., and Weber, R. J.: Reactive oxygen species associated with water-soluble PM2.5 in the southeastern United States: spatiotemporal trends and source apportionment, Atmos. Chem. Phys., 14, 12915-12930, doi:10.5194/acp-14-12915-2014, 2014.

Wängberg, I., Barnes, I., and Becker, K. H.: Product and Mechanistic Study of the Reaction of NO3 Radicals with α-Pinene, Environ. Sci. Technol., 31, 2130-2135, doi:10.1021/es960958n, 1997.

Wayne, R. P., Barnes, I., Biggs, P., Burrows, J. P., Canosamas, C. E., Hjorth, J., Lebras, G., Moortgat, G. K., Perner, D., Poulet, G., Restelli, G., and Sidebottom, H.: THE NITRATE RADICAL - PHYSICS, CHEMISTRY, AND THE ATMOSPHERE, Atmospheric Environment Part a-General Topics, 25, 1-203, doi:10.1016/0960-1686(91)90192-a, 1991.

Weber, R. J., Sullivan, A. P., Peltier, R. E., Russell, A., Yan, B., Zheng, M., de Gouw, J., Warneke, C., Brock, C., Holloway, J. S., Atlas, E. L., and Edgerton, E.: A study of secondary organic aerosol formation in the anthropogenic-influenced southeastern United States, J. Geophys. Res.-Atmos., 112, D13302, doi:13310.11029/12007JD008408, 2007.

Xu, H., Wentworth, P. J., Howell, N. W., and Joens, J. A.: Temperature Dependent Near-UV Molar Absorptivities of Aliphatic Aldehydes and Ketones in Aqueous Solution, Spectrochim. Acta A, 49, 1171-1178, doi:http://dx.doi.org/10.1016/0584-8539(93)80076-M, 1993.

Xu, L., Kollman, M. S., Song, C., Shilling, J. E., and Ng, N. L.: Effects of NOx on the Volatility of Secondary Organic Aerosol from Isoprene Photooxidation, Environ. Sci. Technol., 48, 2253-2262, doi:10.1021/es404842g, 2014.

Xu, L., Suresh, S., Guo, H., Weber, R. J., and Ng, N. L.: Aerosol characterization over the southeastern United States using high resolution aerosol mass spectrometry: spatial and seasonal variation of aerosol composition, sources, and organic nitrates, Atmos. Chem. Phys. Discuss., 15, 10479-10552, doi:10.5194/acpd-15-10479-2015, 2015a.

Xu, L., Guo, H., Boyd, C. M., Klein, M., Bougiatioti, A., Cerully, K. M., Hite, J. R., Isaacman-VanWertz, G., Kreisberg, N. M., Knote, C., Olson, K., Koss, A., Goldstein, A. H., Hering, S. V., de Gouw, J., Baumann, K., Lee, S.-H., Nenes, A., Weber, R. J., and Ng, N. L.: Effects of anthropogenic emissions on aerosol formation from isoprene and monoterpenes in the

southeastern United States, Proceedings of the National Academy of Sciences of the United States of America, 112, 37-42, doi:10.1073/pnas.1417609112, 2015b.

Yeh, G. K., and Ziemann, P. J.: Alkyl Nitrate Formation from the Reactions of C8–C14 n-Alkanes with OH Radicals in the Presence of NOx: Measured Yields with Essential Corrections for Gas–Wall Partitioning, The Journal of Physical Chemistry A, 118, 8147-8157, doi:10.1021/jp500631v, 2014.

Yu, Y., Ezell, M. J., Zelenyuk, A., Imre, D., Alexander, L., Ortega, J., D'Anna, B., Harmon, C. W., Johnson, S. N., and Finlayson-Pitts, B. J.: Photooxidation of alpha-pinene at high relative humidity in the presence of increasing concentrations of NOx, Atmospheric Environment, 42, 5044-5060, doi:10.1016/j.atmosenv.2008.02.026, 2008.

Zaveri, R. A., Berkowitz, C. M., Brechtel, F. J., Gilles, M. K., Hubbe, J. M., Jayne, J. T., Kleinman, L. I., Laskin, A., Madronich, S., Onasch, T. B., Pekour, M. S., Springston, S. R., Thornton, J. A., Tivanski, A. V., and Worsnop, D. R.: Nighttime chemical evolution of aerosol and trace gases in a power plant plume: Implications for secondary organic nitrate and organosulfate aerosol formation, NO3 radical chemistry, and N2O5 heterogeneous hydrolysis, Journal of Geophysical Research-Atmospheres, 115, D12304, doi:10.1029/2009jd013250, 2010.

Zhang, X., Cappa, C. D., Jathar, S. H., McVay, R. C., Ensberg, J. J., Kleeman, M. J., and Seinfeld, J. H.: Influence of vapor wall loss in laboratory chambers on yields of secondary organic aerosol, Proceedings of the National Academy of Sciences of the United States of America, 111, 5802-5807, doi:10.1073/pnas.1404727111, 2014.

Zhang, X., Schwantes, R. H., McVay, R. C., Lignell, H., Coggon, M. M., Flagan, R. C., and Seinfeld, J. H.: Vapor wall deposition in Teflon chambers, Atmos. Chem. Phys., 15, 4197-4214, doi:10.5194/acp-15-4197-2015, 2015.

Zhao, R., Lee, A. K. Y., and Abbatt, J. P. D.: Investigation of Aqueous-Phase Photooxidation of Glyoxal and Methylglyoxal by Aerosol Chemical Ionization Mass Spectrometry: Observation of Hydroxyhydroperoxide Formation, J. Phys. Chem. A, 116, 6253-6263, doi:10.1021/jp211528d, 2012.

Zheng, W., Flocke, F. M., Tyndall, G. S., Swanson, A., Orlando, J. J., Roberts, J. M., Huey, L. G., and Tanner, D. J.: Characterization of a thermal decomposition chemical ionization mass spectrometer for the measurement of peroxy acyl nitrates (PANs) in the atmosphere, Atmos. Chem. Phys., 11, 6529-6547, doi:10.5194/acp-11-6529-2011, 2011.

Ziemann, P. J., and Atkinson, R.: Kinetics, products, and mechanisms of secondary organic aerosol formation, Chemical Society Reviews, 41, 6582-6605, doi:10.1039/c2cs35122f, 2012.

Figure Captions

Figure 1: Schematic of the Georgia Tech Environmental Chamber facility (GTEC).

Figure 2: Time series of the gas-phase organic nitrate species measured by the CIMS and the corresponding aerosol formation measured by HR-ToF-AMS (organics mass) and SMPS (aerosol volume) (Experiment 30 in Table 1). The gas-phase species at *m/z* 356 decreases over the course of the experiment while the species at *m/z* 372 increases steadily.

Figure 3: Aerosol mass yield as a function of organic mass loading for the β-pinene+NO_3 reaction under "RO_2+NO_3 dominant" conditions. The aerosol mass yields obtained in this study are compared to those measured in previous chamber studies by Griffin et al. (1999) and Fry et al. (2009). The aerosol mass yields obtained in this study are fitted using the two-product model proposed previously by Odum et al. (1996). The yield parameters obtained in this study and those from Griffin et al. (1999) are shown in Table 2. In order to better compare the aerosol mass yields obtained in this study to that by Griffin et al. (1999), measurements by Griffin et al. (1999) are adjusted to a temperature of 298K and density of 1.41 g cm^{-3}. The x-axis error bars represent one standard deviation of volume measured by SMPS at peak growth. The y-axis error bars represent uncertainty in yield calculated by an 8% uncertainty in chamber volume, 5% uncertainty in hydrocarbon injection, and one standard deviation of the aerosol volume measured by SMPS at peak growth.

Figure 4: Aerosol mass yield as a function of organic mass loading for the β-pinene+NO_3 reaction under "RO_2+HO_2 dominant" conditions. These aerosol mass yields are compared to the yield curve (solid line) for the NO_3+β-pinene under "RO_2+NO_3 dominant" conditions. The x-axis error bars represent one standard deviation of volume measured by SMPS at peak growth. The y-axis error bars represent uncertainty in yield calculated by an 8% uncertainty in chamber volume, 5% uncertainty in hydrocarbon injection, and one standard deviation of the aerosol volume measured by SMPS at peak growth.

Figure 5: High-resolution aerosol mass spectrum of the SOA formed from the β-pinene+NO_3 reaction under dry, ammonium sulfate seed, and "RO_2+NO_3 dominant" conditions (Experiment 5 in Table 1). The mass spectrum is colored by the ion type to indicate the contribution of each ion type to the mass spectrum. Only ions up to *m/z* 160 are shown as the signals beyond *m/z* 160 are minimal. Ions that contribute significantly to the total signal are also labeled.

Figure 6: Time series of mass concentrations of the major organic families (normalized to the sulfate mass concentration) as measured by the HR-ToF-AMS at RH < 2% under "RO_2+NO_3 dominant" conditions (Experiment 5 in Table 1). The least oxidized organic species (i.e. Family CH) decreases rapidly at the start of the experiment, and has the largest decrease among the three major organic families.

Figure 7: The AMS Nitrate:Org ratio of humid (RH = 50%) experiments normalized to the corresponding dry experiments with same initial β-pinene mixing ratio, five-minute averaged, for "RO_2+NO_3 dominant" experiments. This ratio is referred to as $(Nitrate:Org)_{norm}$ in the main text. For comparison purposes, all data are normalized to the highest $(Nitrate:Org)_{norm}$ ratio.

Figure 8: Generation of gas-phase species with molecular weights (MW) of 215, 229, and 231 amu detected by CIMS (red font), aerosol species with MW = 245 amu in filters analyzed by UHPLC-MS (blue font). Reaction numbers are given in green font and reaction with generic radical $\mathbf{Q}^{\bullet}$ (e.g., NO_3, RO_2, etc.) is used to symbolize any species abstracting hydrogen atoms. Reactions which can be accomplished by any of the radicals present (RO_2, HO_2, NO_3 etc.) are symbolized by reaction with generic radical $\mathbf{L}^{\bullet}$. Reactions enhanced in the RO_2+HO_2 dominant pathway are highlighted in purple.

Figure 9: Ratio of the total areas integrated under UV-visible chromatograms collected at 235 nm (gray bars, ROOR and ROOH) and 270 nm (teal bars, -C=O and -ONO_2) relative to 205 nm for experiments dominated by (left-hand side panel) RO_2+NO_3 reaction and (right-hand side panel) RO_2+HO_2 reaction under both humid and dry conditions.

Figure 10: A comparison of mass spectra obtained from this work and the LO-OOA factor identified from PMF analysis of the HR-ToF-AMS data from the SOAS field campaign. (a) Mass spectrum of the SOA formed from the β-pinene+NO_3 reaction at RH = 70 % under "RO_2+HO_2 dominant" conditions and $(NH_4)_2SO_4$+H_2SO_4 seed (Experiment 34 in Table 1). (b) Mass spectrum for the LO-OOA factor identified from PMF analysis of the SOAS HR-ToF-AMS data (Xu et al., 2015b). The mass spectra are colored by the ion type to indicate their contribution to the mass spectra. Ions $C_5H_7^+$ (*m/z* 67) and $C_7H_7^+$ (*m/z* 91) are distinctive for the β-pinene mass spectrum (Section 5 of main text). To facilitate comparison, *m/z* > 50 have been multiplied by a factor of 3 in the LO-OOA spectrum.

Figure 1:

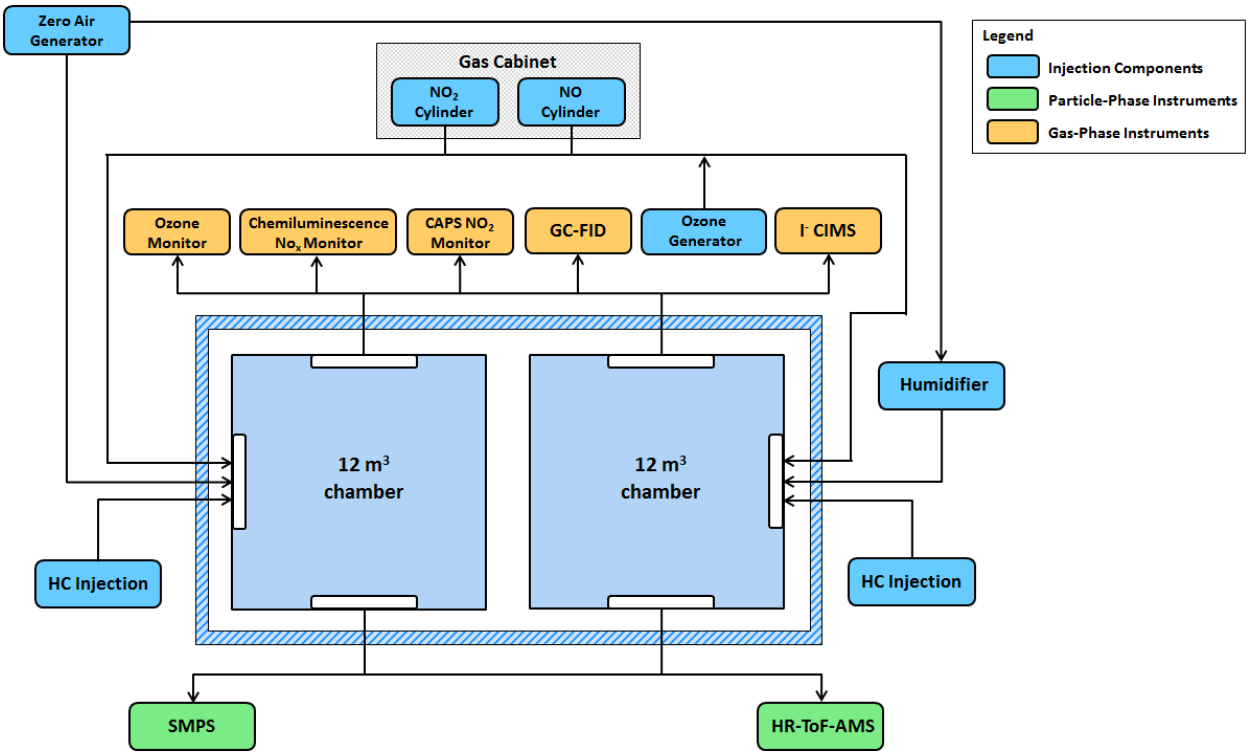
Zero Air Generator
Gas Cabinet
NO_2 Cylinder
NO Cylinder
Legend
Injection Components
Particle-Phase Instruments
Gas-Phase Instruments
Ozone Monitor
Chemiluminescence No_x Monitor
CAPS NO_2 Monitor
GC-FID
Ozone Generator
I^- CIMS
Humidifier
12 m^3 chamber
12 m^3 chamber
HC Injection
HC Injection
SMPS
HR-ToF-AMS

Figure 2:

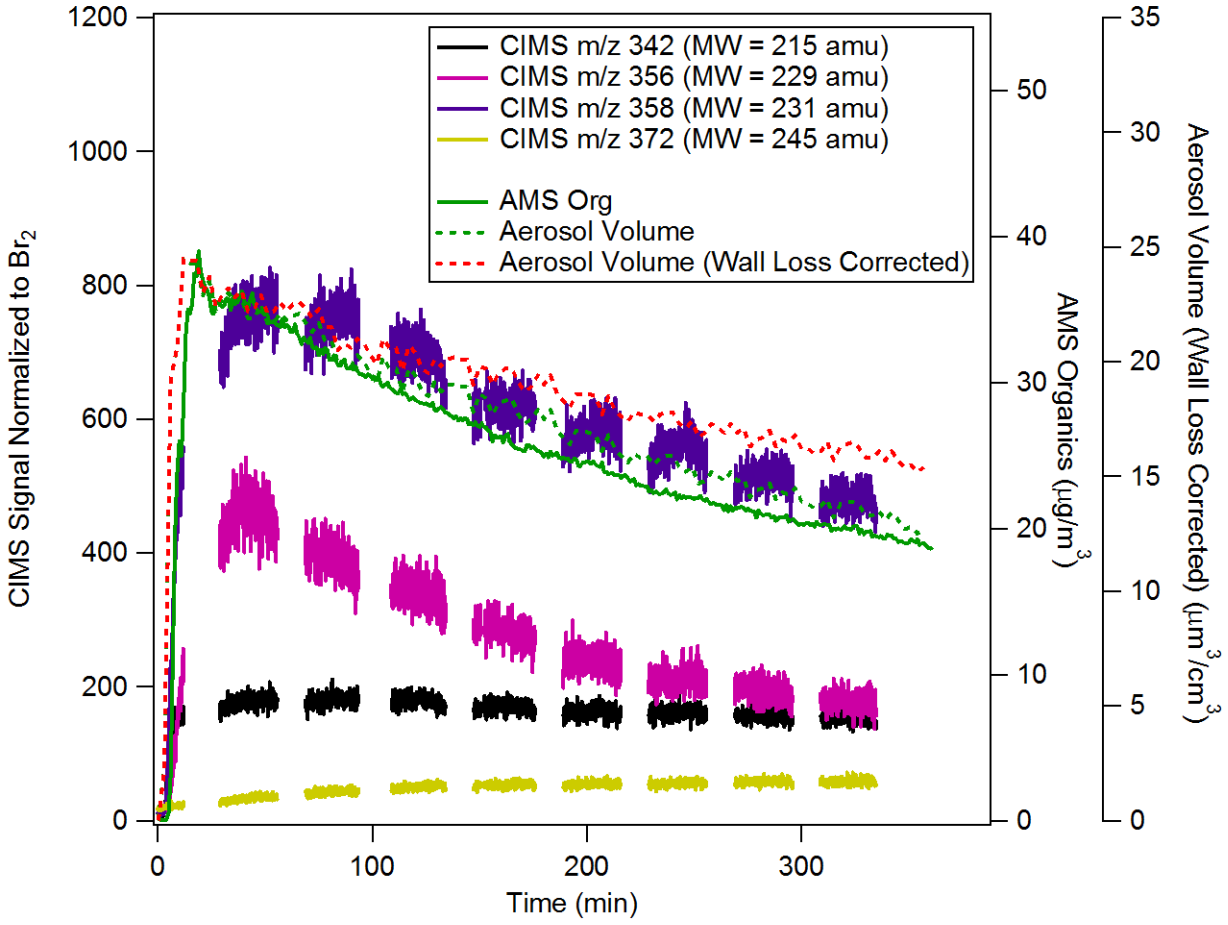
CIMS m/z 342 (MW = 215 amu)
CIMS m/z 356 (MW = 229 amu)
CIMS m/z 358 (MW = 231 amu)
CIMS m/z 372 (MW = 245 amu)
AMS Org
Aerosol Volume
Aerosol Volume (Wall Loss Corrected)
CIMS Signal Normalized to Br2
AMS Organics (μg/m3)
Aerosol Volume (Wall Loss Corrected) (μm3/cm3)
Time (min)
0
200
400
600
800
1000
1200
0
10
20
30
40
50
0
5
10
15
20
25
30
35
0
100
200
300

Figure 3:

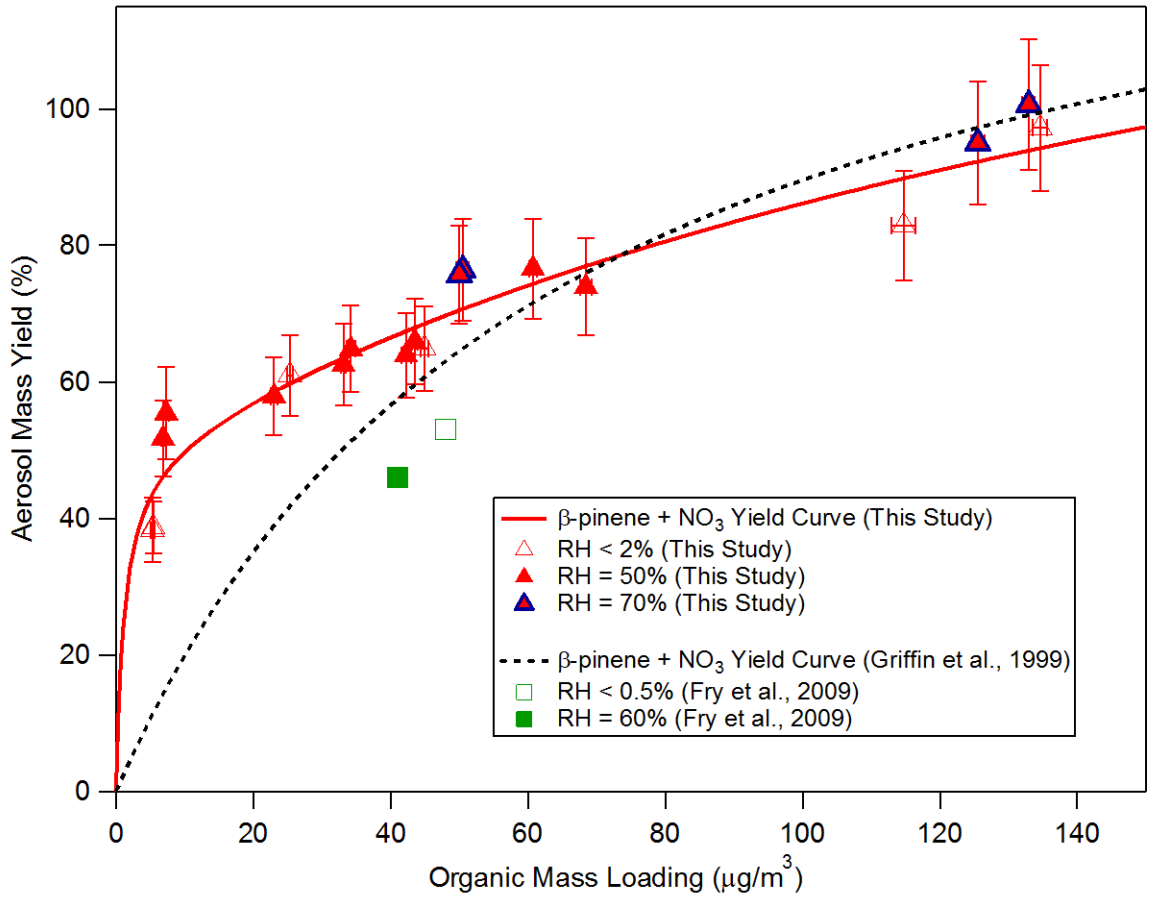
Aerosol Mass Yield (%)
Organic Mass Loading (µg/m3)
β-pinene + NO3 Yield Curve (This Study)
RH < 2% (This Study)
RH = 50% (This Study)
RH = 70% (This Study)
β-pinene + NO3 Yield Curve (Griffin et al., 1999)
RH < 0.5% (Fry et al., 2009)
RH = 60% (Fry et al., 2009)

Figure 4:

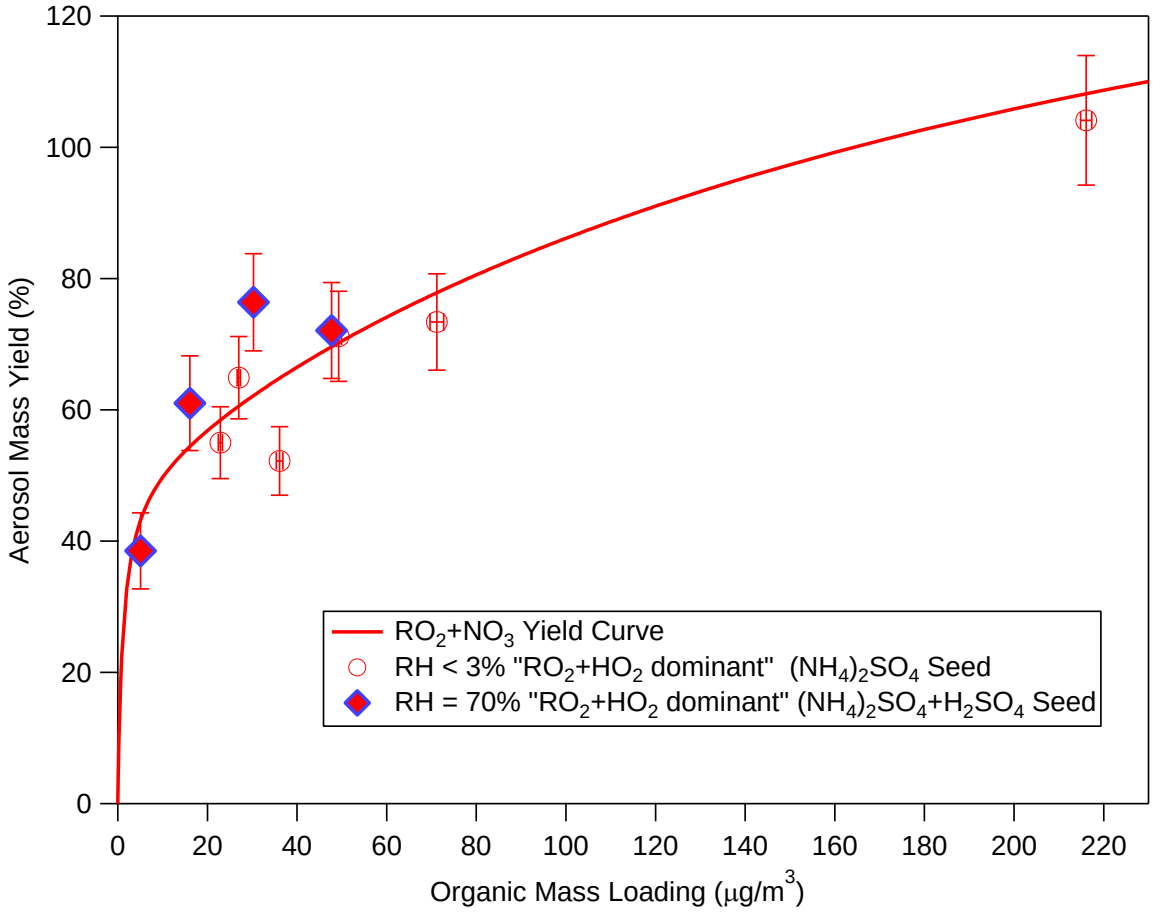
Aerosol Mass Yield (%)
Organic Mass Loading (μg/m3)
RO2+NO3 Yield Curve
RH < 3% "RO2+HO2 dominant" (NH4)2SO4 Seed
RH = 70% "RO2+HO2 dominant" (NH4)2SO4+H2SO4 Seed

Figure 5:

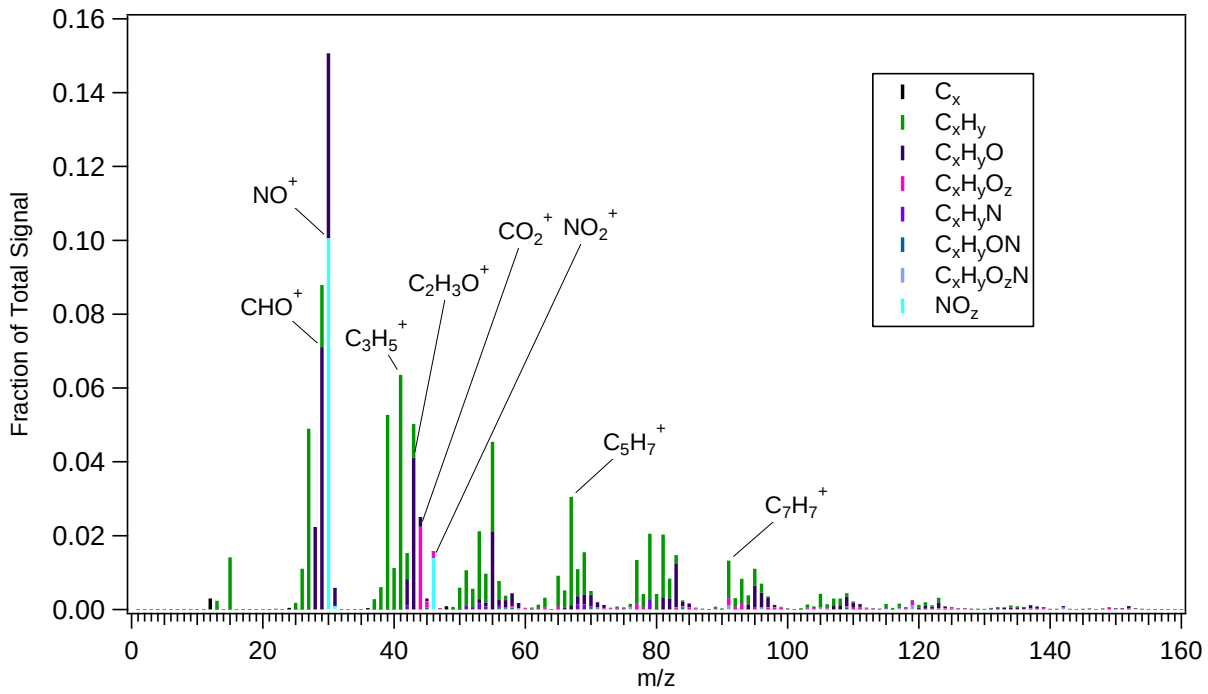
Fraction of Total Signal
m/z
0.00
0.02
0.04
0.06
0.08
0.10
0.12
0.14
0.16
0
20
40
60
80
100
120
140
160
NO+
CHO+
C3H5+
C2H3O+
CO2+
NO2+
C5H7+
C7H7+
Cx
CxHy
CxHyO
CxHyOz
CxHyN
CxHyON
CxHyOzN
NOz

Figure 6:

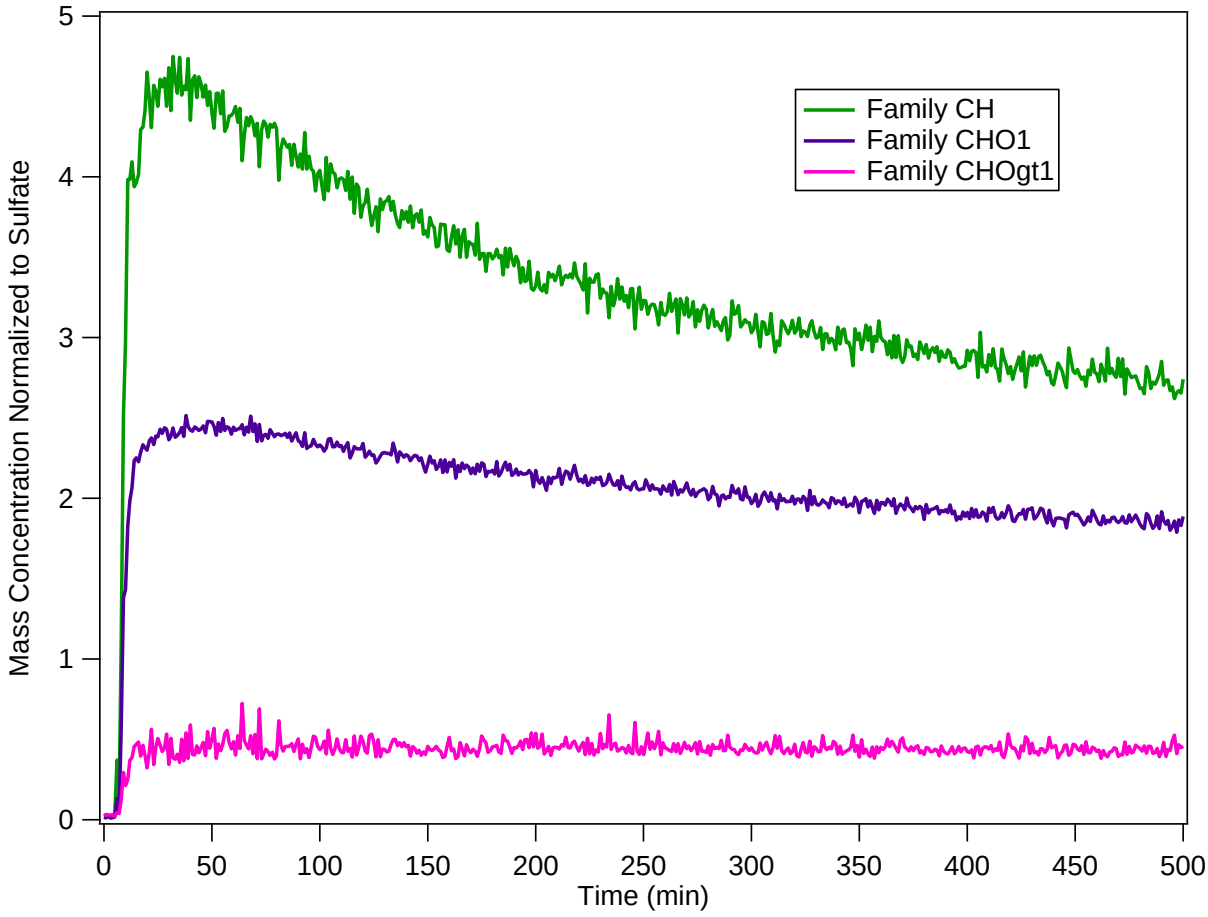
Family CH
Family CHO1
Family CHOgt1
Mass Concentration Normalized to Sulfate
Time (min)
0
1
2
3
4
5
0
50
100
150
200
250
300
350
400
450
500

Figure 7:

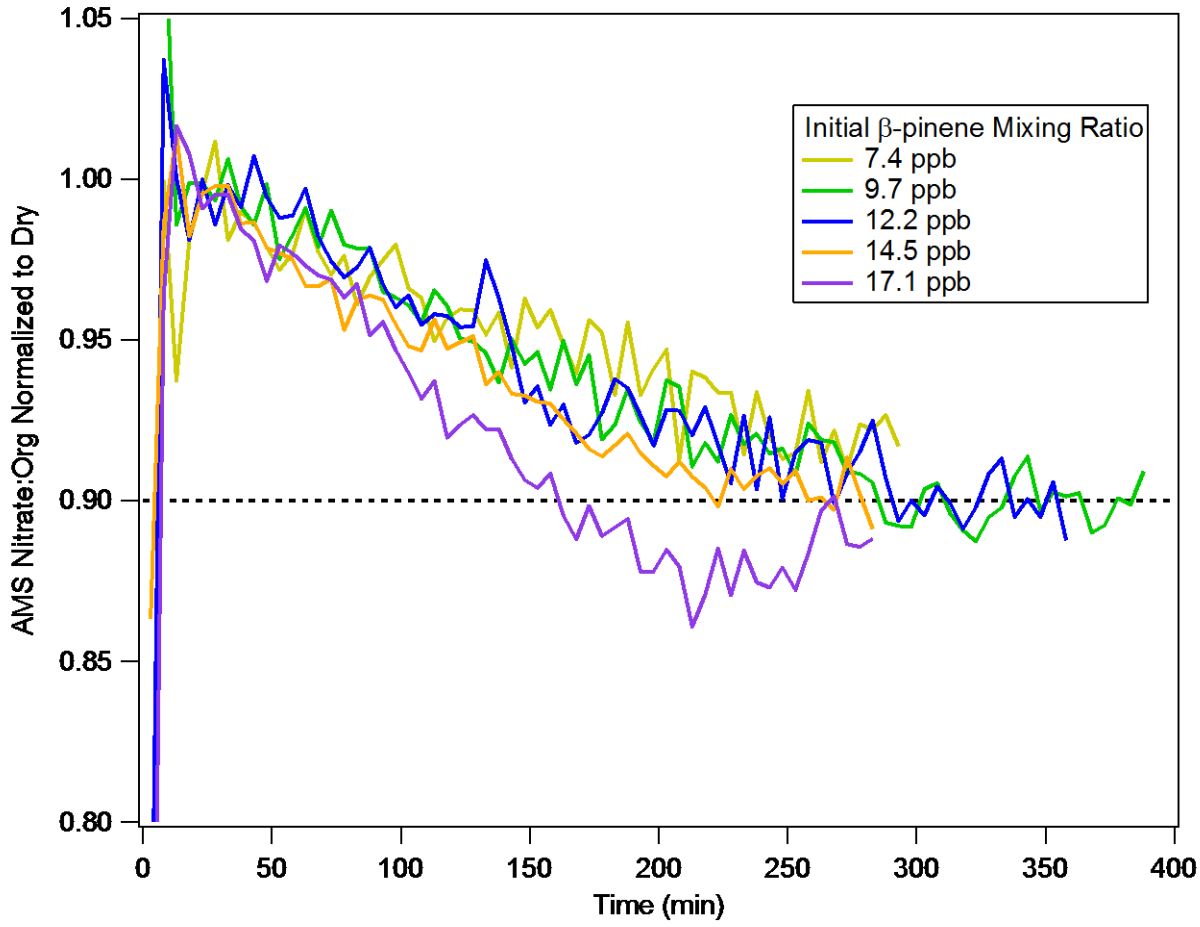
1.05
1.00
0.95
0.90
0.85
0.80
AMS Nitrate:Org Normalized to Dry
0
50
100
150
200
250
300
350
400
Time (min)
Initial β-pinene Mixing Ratio
7.4 ppb
9.7 ppb
12.2 ppb
14.5 ppb
17.1 ppb

1809 Figure 8:

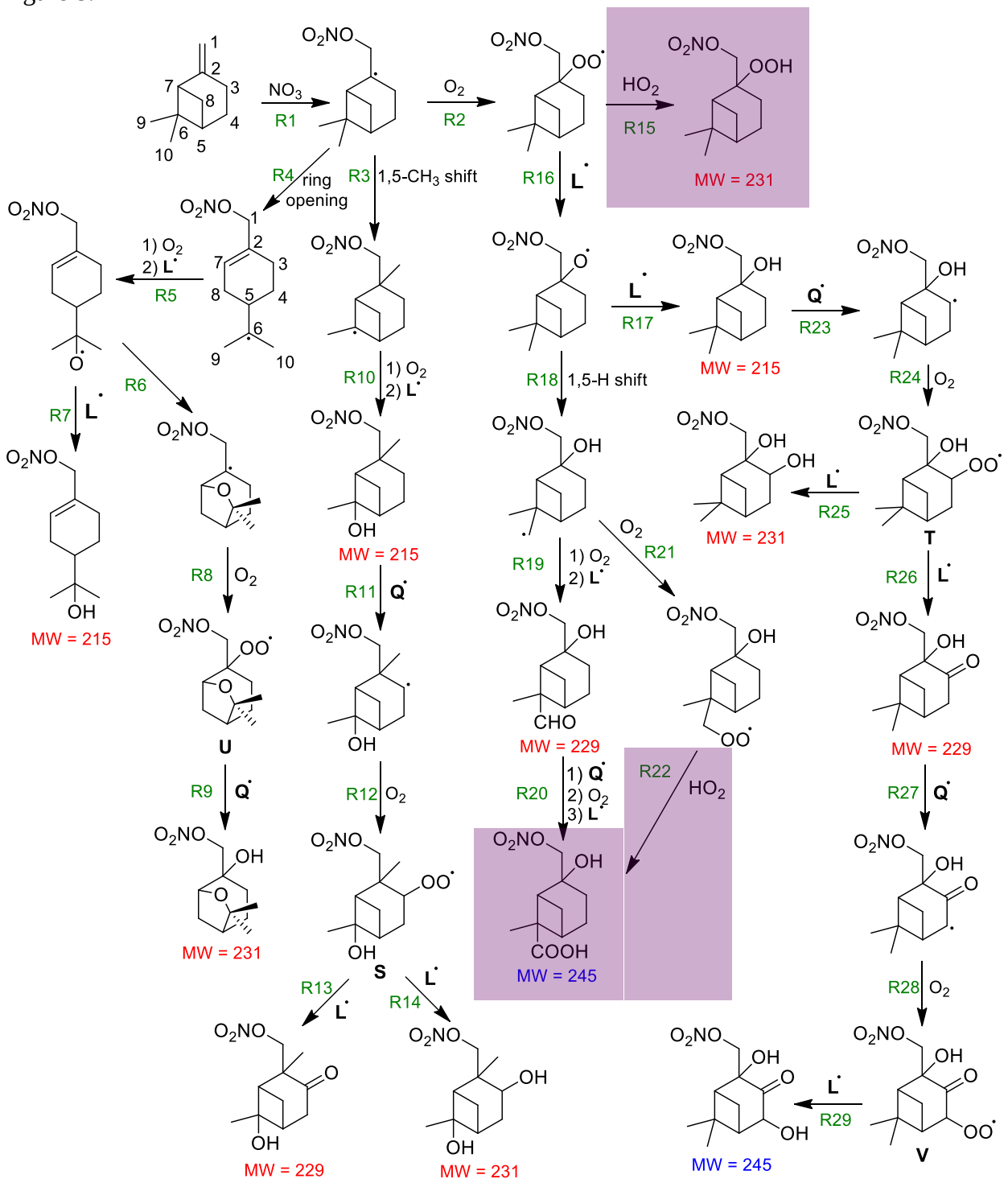

1810

1811

1812

1813

1814

Figure 9:

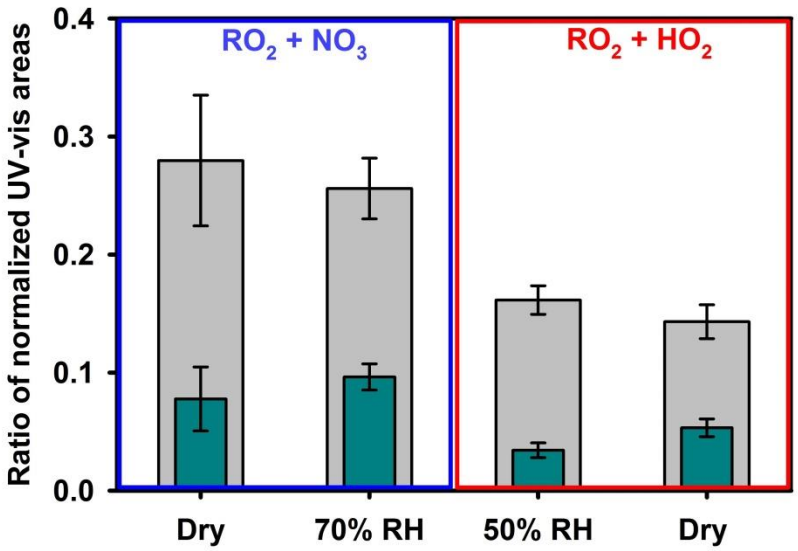
Ratio of normalized UV-vis areas
0.4
0.3
0.2
0.1
0.0
RO2 + NO3
RO2 + HO2
Dry
70% RH
50% RH
Dry

1827 Figure 10:

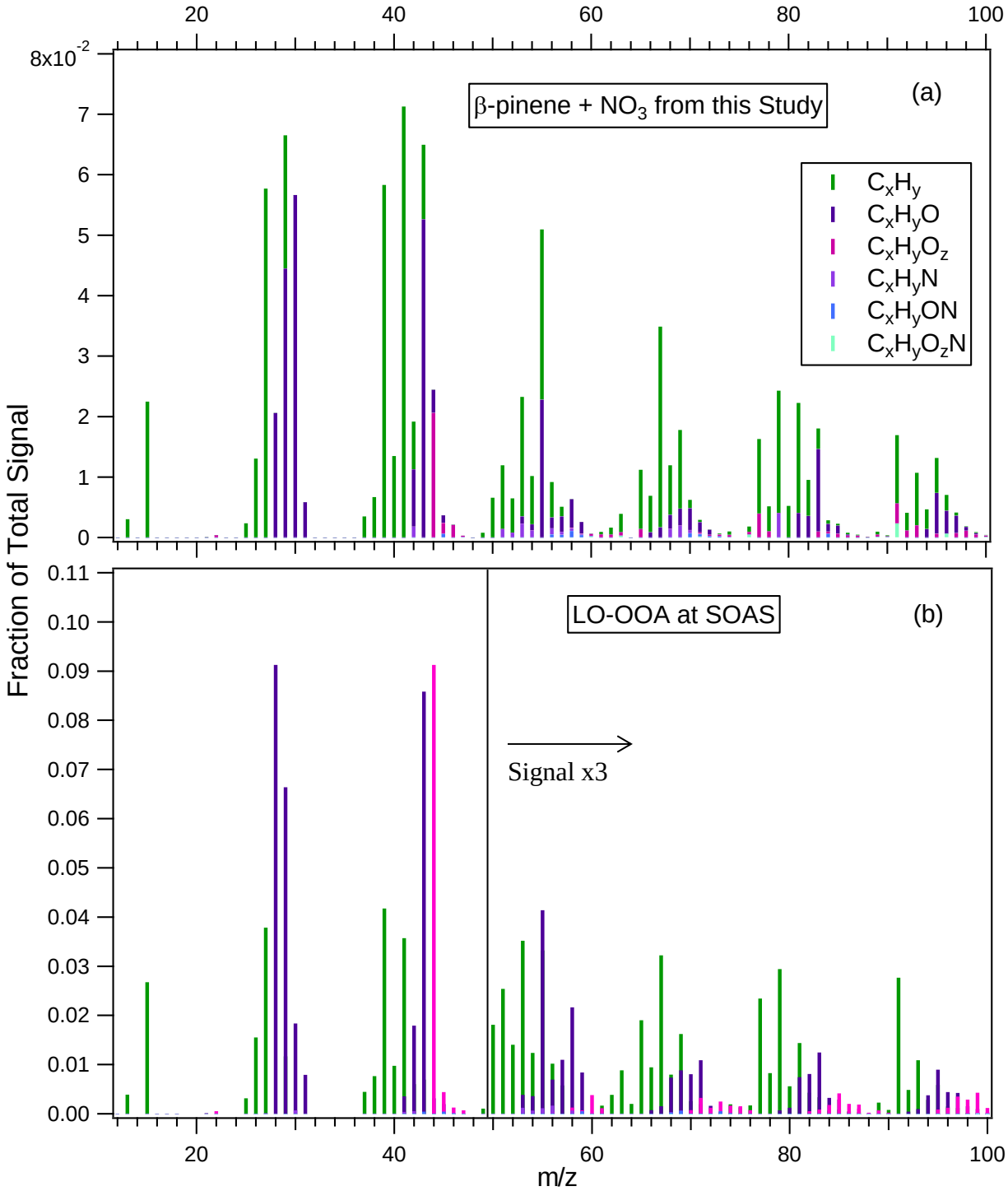

1828

1829 Table 1: Experimental conditions and aerosol mass yields for all experiments
1830

Experiment	RH (%)	Condition	Seed	ΔHC^c (ppb)	ΔHC^c ($\mu g\ m^{-3}$)	$\Delta M_o{}^d$ ($\mu g\ m^{-3}$)	Mass Yield (%)
1	< 2	RO_2+NO_3	AS[a]	2.5±0.2	13.8±1.3	5.3±0.41	38.3±5.5
2	< 2	RO_2+NO_3	AS	2.5±0.2	13.8±1.3	5.4±0.15	38.7±4.0
3	< 2	RO_2+NO_3	AS	7.4±0.7	41.5±3.9	25.3±0.54	61.0±6.0
4	< 2	RO_2+NO_3	AS	9.9±0.9	55.4±5.2	--[e]	--
5	< 2	RO_2+NO_3	AS	12.4±1.2	69.2±6.5	--	--
6	< 2	RO_2+NO_3	AS	12.4±1.2	69.2±6.5	44.9±0.73	64.9±6.3
7	< 2	RO_2+NO_3	AS	14.9±1.4	83.0±7.8	--	--
8	< 2	RO_2+NO_3	AS	17.4±1.6	96.9±9.1	--	--
9	< 2	RO_2+NO_3	AS	24.8±2.4	138.4±13.1	134.6±1.51	97.2±9.3
10	< 2	RO_2+NO_3	AS	24.8±2.4	138.4±13.1	114.7±2.51	82.9±8.2
11	51	RO_2+NO_3	AS	2.4±0.2	13.2±1.2	7.3±0.57	55.4±8.2
12	50	RO_2+NO_3	AS	2.4±0.2	13.2±1.2	6.8±0.36	51.7±6.3
13	49	RO_2+NO_3	AS	7.1±0.7	39.6±3.7	23.0±0.65	57.9±6.0
14	49	RO_2+NO_3	AS	9.5±0.9	52.8±5.0	34.2±0.89	64.8±6.6
15	51	RO_2+NO_3	AS	9.5±0.9	52.8±5.0	33.1±0.56	62.5±6.1
16	50	RO_2+NO_3	AS	11.9±1.1	66.1±6.2	43.5±0.60	65.9±6.4
17	50	RO_2+NO_3	AS	11.9±1.1	66.1±6.2	42.2±0.98	63.9±6.4
18	51	RO_2+NO_3	AS	14.2±1.3	79.3±7.5	60.7±0.83	76.6±7.4
19	51	RO_2+NO_3	AS	16.6±1.6	92.5±8.7	68.4±1.26	73.9±7.2
20	71	RO_2+NO_3	AS	11.9±1.1	66.1±6.2	50.5±1.32	76.4±7.8
21	70	RO_2+NO_3	AS	11.9±1.1	66.1±6.2	50.0±0.44	75.7±7.2
22	72	RO_2+NO_3	AS	23.7±2.2	132.1±12.5	125.5±1.35	95.0±9.0
23	68	RO_2+NO_3	AS	23.7±2.2	132.1±12.5	132.9±1.33	100.6±9.5
24	51	RO_2+NO_3	AS+SA[b]	7.1±0.7	39.6±3.7	25.5±0.69	64.4±6.6
25	50	RO_2+NO_3	AS+SA	11.9±1.1	66.1±6.2	46.4±1.10	70.4±6.8
26	51	RO_2+NO_3	AS+SA	16.6±1.6	92.5±8.7	74.4±1.23	80.5±7.7
27	< 3	RO_2+HO_2	AS	7.4±0.7	41.5±3.9	27.0 ±0.54	64.9±6.4
28	< 3	RO_2+HO_2	AS	7.4±0.7	41.5±3.9	22.9±0.71	55.0±5.8
29	< 3	RO_2+HO_2	AS	12.4±1.2	69.2±6.5	49.3±0.97	71.2±7.1
30	< 3	RO_2+HO_2	AS	12.4±1.2	69.2±6.5	36.1±1.17	52.2±5.6
31	< 2	RO_2+HO_2	AS	17.4±1.6	96.9±9.1	71.2±2.32	73.4±7.8
32	< 3	RO_2+HO_2	AS	37.3±3.5	207.6±19.6	216.1±1.96	104.1±9.9
33	49	RO_2+HO_2	AS	35.6±3.4	198.2±18.7	147.8±1.42	74.6±7.1
34	69	RO_2+HO_2	AS+SA	2.4±0.2	13.2±1.2	5.1±0.59	38.5±8.1
35	69	RO_2+HO_2	AS+SA	4.7±0.4	26.4±2.5	16.1±1.14	61.0±9.0
36	66	RO_2+HO_2	AS+SA	7.1±0.7	39.6±3.7	30.3±0.71	76.4±7.8
37	66	RO_2+HO_2	AS+SA	11.9±1.1	66.1±6.2	47.7±1.77	72.1±8.1
38	< 1	RO_2+NO_3	None	12.4±1.2	69.2±6.5	42.3±0.46	61.1±5.8
39	50	RO_2+NO_3	None	11.9±1.1	66.1±6.2	44.3±0.34	67.0±6.4
40	<2	RO_2+HO_2	None	12.4±1.2	69.2±6.5	18.7±0.51	27.0±2.8
41	66	RO_2+HO_2	None	11.9±1.1	66.1±6.2	28.5±0.60	43.1±4.2

42	50	RO_2+HO_2	None	11.9±1.1	66.1±6.2	18.4±0.34	27.8±2.7
43	<2	RO_2+HO_2	AS*	12.4±1.2	69.2±6.5	33.6±0.79	48.5±4.9
44	68	RO_2+HO_2	AS+SA*	11.9±1.1	66.1±6.2	46.6±0.86	70.6±7.0
45	66	RO_2+HO_2	AS+SA*	11.9±1.1	66.1±6.2	44.5±0.87	67.3±6.7

*Experiments with seed concentrations greater than the typical seed concentrations for investigating vapor wall loss effects

[a]$(NH_4)_2SO_4$ Seed

[b]$(NH_4)_2SO_4+H_2SO_4$ Seed

[c]Uncertainties in hydrocarbon concentration are calculated from an 8% uncertainty in chamber volume and 5% uncertainty in hydrocarbon mass

[d]Uncertainties in aerosol mass loading are calculated from one standard deviation of aerosol volume as measured by the SMPS

[e]"--" denotes experiments where there is no SMPS data

Table 2: Fit parameters for two-product model proposed by Odum et al. (1996)

	α_1	K_1	α_2	K_2
β-pinene+NO_3 (this study)	1.187	0.004546	0.496	0.880
Griffin et al. (1999)	1.464	0.0158		

Table 3: Coefficients for the Volatility Basis Set Proposed by Donahue et al. (2006)

	Saturation Vapor Pressure, C* (μg m^{-3})			
	0.1	1	10	100
β-pinene+NO_3 (this study)	0.373	0.033	0.000	0.941
Griffin et al. (1999)	0.000	0.000	0.301	1.204